A gridded dataset of consumptive water footprints, evaporation, transpiration, and associated benchmarks related to crop production in China during 2000-2018

Wei Wang[1,2,3], La Zhuo[1,2,3,4]*, Xiangxiang Ji[5], Zhiwei Yue[5], Zhibin Li[1,2,3], Meng Li[5], Huimin Zhang[5], Rong Gao[5], Chenjian Yan[5], Ping Zhang[5], Pute Wu[2,4]*

[1]The Research Center of Soil and Water Conservation and Ecological Environment, Chinese Academy of Sciences and Ministry of Education, Yangling, Shaanxi 712100, China

[2]Institute of Soil and Water Conservation, Chinese Academy of Sciences and Ministry of Water Resources, Yangling, Shaanxi 712100, China

[3]University of Chinese Academy of Sciences, Beijing 100049, China

[4]College of Soil and Water Conservation Science and Engineering, Northwest A&F University, Yangling, Shaanxi 712100, China

[5]College of Water Resources and Architectural Engineering, Northwest A&F University, Yangling, Shaanxi 712100, China

Correspondence to: La Zhuo (zhuola@nwafu.edu.cn; lzhuo@ms.iswc.ac.cn), Pute Wu (gjzwpt@vip.sina.com).

Abstract. Evapotranspiration over crop growth period, also referred to as the consumptive water footprint of crop production (WFCP), is an essential component of the hydrological cycle. However, the existing high-resolution consumptive WFCP datasets do not distinguish between soil evaporation and crop transpiration and disregard the impacts of different irrigation practices. This restricts the practical implementation of existing WFCP datasets for precise crop water productivity assessments, agricultural water-saving evaluations, the development of sustainable irrigation techniques, cropping structure optimisation, and crop-related interregional virtual water trade analysis. This study establishes a 5-arcmin gridded dataset of monthly green and blue WFCP, evaporation, transpiration, and associated unit WFCP benchmarks for 21 crops grown in China during 2000-2018. The data simulation was based on calibrated AquaCrop modelling under furrow-, sprinkler-, and micro-irrigated as well as rainfed conditions. Data quality was validated by comparing the current results with multiple public datasets and remote-sensing products. The improved gridded WFCP dataset is available at https://doi.org/10.5281/zenodo.7756013 (Wang et al., 2023) and effectively compensated for the gaps in the existing datasets through: (i) revealing the intensity, structure, and spatiotemporal evolution of both productive and non-productive blue and green water consumption on a monthly scale, and (ii) including crop-by-crop unit WFCP benchmarks according to climatic zones.

1 Introduction

The grain production potential of irrigated agriculture can effectively cope with the pressure that population growth places on the food supply (Wada et al., 2013; Haddeland et al., 2014; Rosa et al., 2020; Puy et al., 2021; Wang et al., 2021) and

restrain the encroachment of cultivated land on natural regions (Tilman et al., 2011; Brown and Pervez, 2014; Jägermeyr et al., 2017; Puy et al., 2020). Currently, irrigation accounts for more than 70% of worldwide blue water withdrawals (FAO, 2020) and 90% of global water consumption (Döll, 2009). Irrigated cropland increases the soil water content and releases water vapour into the atmosphere, leading to an alteration in the hydrological cycle (Rodell et al., 2009; Elliott et al., 2014; Leng et al., 2014). Meanwhile, water scarcity is expected to increase in more than 80% of global farmlands, together with the increasingly serious threats on sufficient agricultural water supply by the competition for water among sectors (Yin et al., 2017; Pastor et al., 2019; Liu et al., 2022). Apparently, accurate assessment of water consumption on irrigated and rainfed farmlands is crucial for identifying water-use hotspots and ensuring a stable food supply, particularly in the context of climate change.

The consumptive water footprint of crop production (WFCP) measures the consumption of blue water (i.e., irrigation water extracted from surface and groundwater) and green water (i.e., soil water directly from rainfall) during the crop growth period (Hoekstra and Chapagain, 2008; Hoekstra et al., 2011; Hoekstra, 2013), permitting a unified evaluation of the water consumption of irrigated and rainfed crops (Lovarelli et al., 2016). The most widely used WFCP database is the WaterStat (Hoekstra and Mekonnen, 2012). It covers the WFCP of a wide variety of crops, crop derivatives, and biofuels, with data resolution at national, watershed, and county spatial scales, but it only contains 10-year averages for 1996-2005 (WFN, 2022). The CWASI database established by Tamea et al. (2021) fills the resultant gap concerning the interannual evolution of WFCP data through a fast-track approach (Tuninetti et al., 2017) at the national scale, suggesting that there is significant interannual variation in the water footprint per unit mass of crop production (uWFCP), which should be taken into account in analyses and applications. However, none of the aforementioned studies have considered intra-annual variations or intra-national differences in agricultural water consumption. Considering that disparities in space and time in the WFCP and uWFCP may have various effects on the formulation of water management measures. Such changes must be evaluated to provide a reference for seasonal water shortages (Hoekstra, 2013; Zhuo et al., 2016c).

Numerous studies have assessed the blue and green WFCP of specific crops at finer spatial and temporal resolutions using the agro-hydrological models including CROPWAT (Mekonnen and Hoekstra, 2011; Tuninetti et al., 2015), GEPIC (Liu et al., 2007), GCWM (Siebert and Döll, 2010), LPJmL (Fader et al., 2011), and AquaCrop (Zhuo et al., 2016b; Wang et al., 2019). Utilising the WATNEEDs model, Chiarelli et al. (2020) produced the first dataset to record global monthly blue and green water requirements of producing 23 crops at a 5 arcmin scale. They found that green water accounts for 84% of the considered global crop water requirements. However, the actual water consumption during crop production is frequently less than the predicted water requirement owing to soil water deficit, insufficient precipitation, and differences in field management (Long and Singh, 2013; Fisher et al., 2017). Furthermore, the aforementioned datasets ignore the non-negligible differences between the WFCP when using different water supply modes or irrigation practices and do not distinguish between the blue and green

water consumption of two independent processes, namely soil evaporation (that is extravagant water consumption) and crop transpiration. In summary, the limitations of existing WFCP databases mean that they cannot be used to evaluate the effect of implementing water-saving irrigation practices on the spatiotemporal distribution of agricultural water consumption at a large regional scale (Wang et al., 2019). Moreover, the lack of information on extravagant water consumption of crops in terms of the water sources and the spatiotemporal distribution hinders the precise implementation of water-saving agricultural policies and technologies (Jung et al., 2010; Lian et al., 2018).

To fill the abovementioned gaps in existing WFCP datasets, we developed a gridded dataset comprising monthly green and blue WFCP, evaporation and transpiration, and associated uWFCP benchmarks for 21 crops grown in China during 2000-2018. A self-sufficiency-oriented food policy has fuelled the explosive growth of water-saving irrigated farmlands in China in recent decades (SCIO, 1996; Ghose, 2014), with water-saving irrigated areas increasing by 5,698 kha from 2000 to 2018 (representing 12% of the total irrigated area in 2018) (NBSC, 2022). The current study followed the WFN accounting framework (Hoekstra et al., 2011) and used FAO AquaCrop Plug-In program V6.0 to simulate the monthly WFCP at a resolution of 5 arcmin. The considered 21 crops account for 83% of national sown areas and 75% of national crop production in China (NBSC, 2022). The dataset differs from the others in four aspects: (i) It evaluated the effects of different water supply modes (irrigated or rain-fed) and irrigation practices (furrow, sprinkler, and micro-irrigation) on water consumption throughout the crop growth period. (ii) It distinguished between monthly blue and green water consumption via soil evaporation and crop transpiration. (iii) The dataset encompassed both the WFCP in $m^3\ yr^{-1}$ and the uWFCP in $m^3\ ton^{-1}$. (iv) It identified uWFCP benchmarks that differentiated between various climatic zones and irrigation practices. The data quality was verified through its comparison with available public databases and remote sensing products.

2 Data and methods

Three main steps were followed to create and validate the WFCP dataset under various water supply modes and irrigation practices during 2000-2018 (Fig. 1).

Step 1: Data preparation. We collected, verified, and inverted data on the yearly planting area of each crop under various water supply modes and irrigation practices at a resolution of 5 arcmin. The AquaCrop simulation required monthly precipitation, temperature, reference evapotranspiration (ET_0), and CO_2 datasets. The calibrated crop parameters were obtained from the published literature.

Step 2: Water footprint simulation. The AquaCrop model was run with daily steps to simulate soil evaporation, crop transpiration, and crop yield during the growth period of crops. The WFCP and uWFCP were calculated for different water

supply modes and irrigation practices using a spatial resolution of 5 arcmin and a temporal resolution of months (Zhuo et al., 2016c; Wang et al., 2019).

Step 3: Data validation. The simulation results were verified by comparing them with remote sensing products of actual evapotranspiration (Cheng et al., 2021) and publicly accessible WFCP datasets (Mekonnen and Hoekstra, 2011; Zhuo et al., 2016a; Chiarelli et al., 2020).

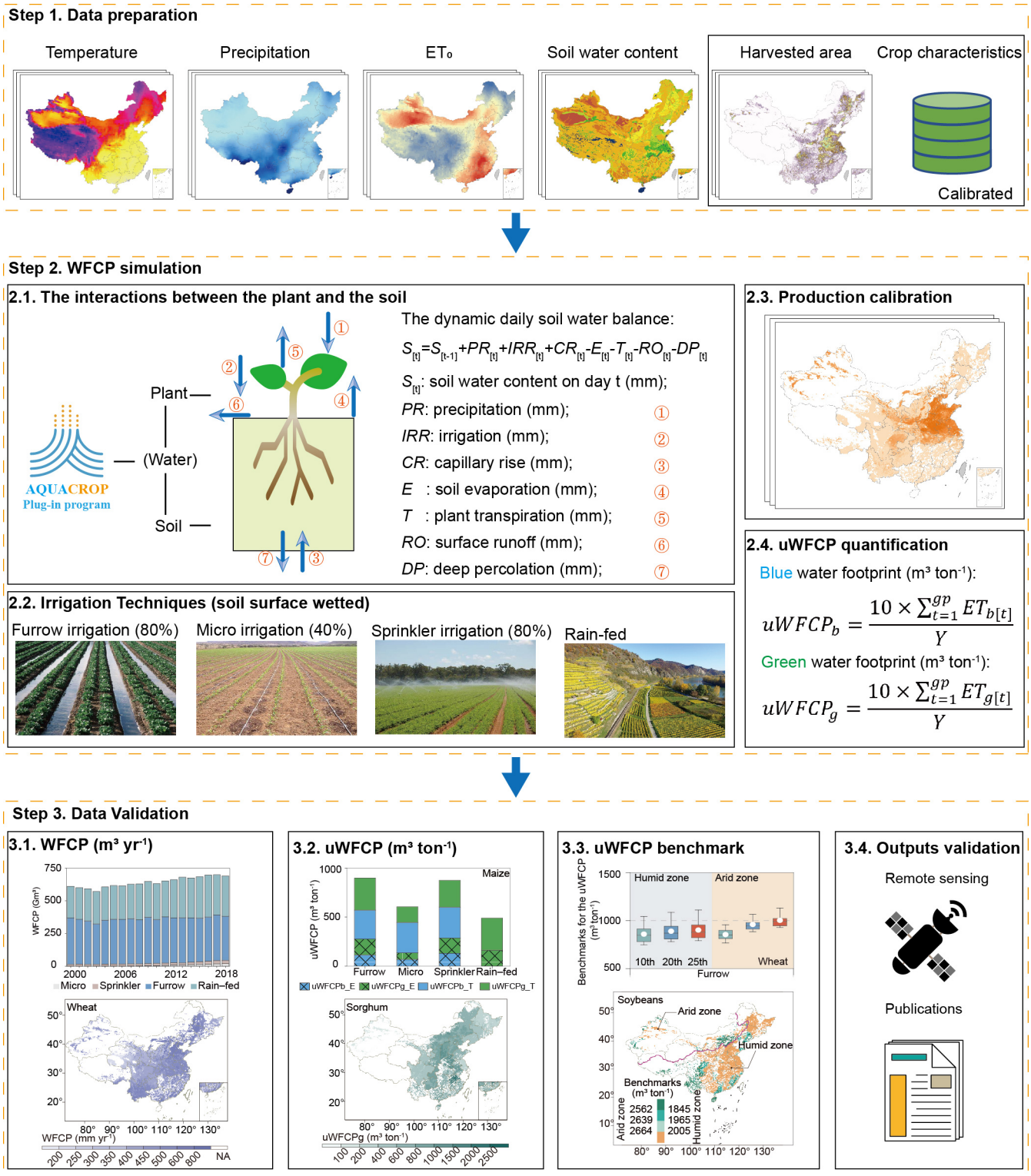

Figure 1. Three main steps for quantifying the water footprint of crop production.

2.1 Data sources

2.1.1 Crop planting area and production

The irrigated and rain-fed areas of each crop from 2001 to 2018 were assigned at a resolution of 5 arcmin according to the base map for the year 2000 obtained from the MIRCA2000 dataset (Portmann et al., 2010) and interannual changes per province extracted from the China Statistical Yearbook (NBSC, 2022). At the provincial scale, irrigation data from 2000-2018 were spatially divided into the proportional areas in which furrow, sprinkler, and micro-irrigation was used for each crop, retrieving data from the statistical yearbook (CAMIYC, 2022). Due to the lack of data in this regard, all vegetables were assumed to be grown under irrigation as based on agricultural practice. Further details about the planting area data selection have been provided in the Supplementary data and methods. The national production data for tomatoes and cabbage were derived from the Food and Agriculture Organization dataset (FAO, 2022) and was proportionally allocated to vegetable production by provinces. Production data for the remaining crops were obtained from the NBSC (2022).

2.1.2 Meteorological and soil data

The monthly data for precipitation, minimum and maximum temperature, and reference evapotranspiration were obtained from the Climatic Research Unit Time-Series 4.06 dataset (Harris et al., 2020). All meteorological data were resampled to a 5 arcmin spatial resolution using the ArcGIS mapping platform. Atmospheric CO_2 concentration data were acquired from the Mauna Loa Observatory in Hawaii (Tans and Keeling, 2020). Soil texture data were obtained from the International Soil Reference and Information Centre (ISRIC) soil profile database (Dijkshoorn et al., 2008). Soil water content data were obtained from the ISRIC World Inventory of Soil Emission Potentials database (Batjes, 2012). Table 1 summarizes the data sources.

Table 1. Inventory of data sources.

Variables	Data source	Spatial resolution	Period	Data link
Irrigated and rainfed crop areas	MIRCA 2000	5 arcmin	2000-2018	https://www.uni-frankfurt.de/45218031/Data_download_center_for_MIRCA2000
Crop production, yield and harvested areas	NBSC	Provincial	2000-2018	https://data.stats.gov.cn/adv.htm?m=advquery&cn=E0103
Production of vegetables	FAOSTAT	National	2000-2018	https://www.fao.org/faostat/en/#data/QV
Area of different irrigation techniques	CAMIY	Provincial	2000-2018	https://data.cnki.net/Trade/yearbook/single/N2021040192?zcode=Z032
Meteorological data	CRU TS v. 4.03	30 arcmin	2000-2018	https://crudata.uea.ac.uk/cru/data/hrg/

CO_2 concentration	NOAA	Average	2000-2018	https://gml.noaa.gov/ccgg/trends/data.html
Soil texture	ISRIC	1 arcmin	-	https://data.isric.org/geonetwork/srv/eng/catalog.search#/metadata/2919b1e3-6a79-4162-9d3a-e640a1dc5aef
Initial soil moisture content	ISRIC	5 arcmin	-	https://data.isric.org/geonetwork/srv/eng/catalog.search#/metadata/82f3d6b0-a045-4fe2-b960-6d05bc1f37c0

Note: "-" means constant values.

2.1.3 Crop characteristics

The characteristics of crops selected for this study are listed in Table 2. Due to differences in their phenology, wheat, maize, barley, and rapeseed had two sowing periods, whereas rice had three sowing periods across the study's time frame. The growth period of all crops was divided into four stages based on their growth characteristics (Allen et al., 1998; Vanuytrecht et al., 2014): the initial (L1), crop development (L2), mid-season (L3), and late-season (L4) growth stages. Crop planting dates were retrieved from Chen et al. (1995). The phenology selection procedure is delineated and the sensitivity analysis of WFCP to phenology are performed within the phenology selection of Supplementary data and methods. The reference harvest index (HI_0) from Xie et al. (2011) and Zhang and Zhu (1990), and crop growth stages and maximum root depth from Allen et al. (1998) and Hoekstra and Chapagain (2006).

Table 2. Crop characteristics for the 21 crops in China.

Crop class	Crop code	Planting date	Length of crop development stage (day)				Root deeps (m)		WP*	HI_0
			L1	L2	L3	L4	Irrigated	Rainfed		
Wheat	1									
Spring wheat		15th Mar	20	25	60	30	1	1.5	15	39
Winter wheat		15th Oct	30	140	40	30	1.5	1.8	15	40
Maize	2									
Spring maize		15th Apr	30	40	50	30	1	1.7	33.7	44
Summer maize		1st Jun	20	35	40	30	1	1.7	33.7	43
Rice	3									
Early rice		15th Mar	30	30	30	30	0.5		19	44
Mid rice		15th Apr	30	30	60	30	0.5		19	44
Late rice		15th Jul	30	30	70	40	0.5		19	44
Sorghum	4	1st May	20	35	45	30	1	2	33.7	39
Millet	5	15th Apr	15	55	40	20	1	1.5	32	47
Barley	6									
Spring barley		15th Apr	15	35	50	30	1	1.5	15	39
Winter barley		25th Oct	20	110	40	35	1	1.5	15	39

Soybeans	7	1st Jun	20	40	60	30	0.6	1.3	15	44
Potatoes	8	1st May	25	30	45	30	0.4	0.6	18	69
Sweet potatoes	9	1st May	20	30	60	40	1	1.5	18	59
Cotton	10	1st Apr	30	50	55	45	1	1.7	15	38
Sugar cane	11	1st Feb	30	50	180	60	1.2	2	30	60
Sugar beets	12	15th Apr	50	40	50	40	0.7	1	17	71
Groundnuts	13	15th Apr	10	80	35	25	0.5	1	17	43
Rapeseed	14									
Spring rapeseed		15th Apr	6	69	20	36	0.8	1.5	17	32
Winter rapeseed		30th Sep	6	148	20	36	0.8	1.5	17	32
Sunflower	15	15th Apr	25	35	45	25	0.8	1.5	18	31
Tomatoes	16	15th Jan	30	40	40	25	0.7	1.5	18	40
Apple	17	1st Mar	30	50	130	30	1	2	20	20
Tea	18	15th Feb	120	60	180	5	0.9	0.9	17	5
Tobacco	19	15th May	20	30	30	30	0.8	0.8	17	61
Cabbage	20	5th Jul	40	60	50	15	0.5	0.8	15	67
Grapes	21	1st Apr	30	60	40	80	1		17	2

2.2 Methods

2.2.1 Spin-up for the model

To establish the initial soil moisture content at the beginning of the growing season, the method and assumptions proposed by Siebert and Döll (2010) were adopted. Following their approach, the initial soil moisture content was generated utilizing the maximum soil moisture content of rainfed fallow land in the two years preceding the planting period. The initial soil moisture at the start of the growing period is assumed as green water. Such settings and assumptions have been extensively applied and with acceptable uncertainties (Chiarelli et al., 2020; Hoogeveen et al., 2015).

2.2.2 Parameterization of perennial crop

In AquaCrop, the simulated annual crops are programmed to die at the harvest stage, signifying the completion of their life cycle, upon which their biomass is reduced to zero. This stands in contrast to perennial plants such as tea and apple trees, where the harvest of fruits does not result in the complete loss of the standing biomass. To accommodate the simulation of perennial crops in AquaCrop, the model is used differently than the normal model set-up. We attempted to simulate the perennial crops by simulating the foliage, twigs and stem of the plants following Poppe (2016). These components are considered the annual portion of perennial crops within the scope of this study. The remaining biomass, including major branches, is assumed to remain constant once the tree matures. Additionally, there will also be no root development for the

crop. Since yield is a direct function of biomass and harvest index, adjustments are made to the harvest index to reflect its applicability to foliage, twigs and stem biomass, rather than the whole biomass. Similar to other crops, the evapotranspiration of perennial crops is directly associated with the canopy cover.

2.2.3 Calculation of uWFCP

The blue and green uWFCP were obtained from the blue and green components of the WFCP (evapotranspiration during the crop growth period) in relation to the crop yield (Hoekstra et al., 2011).

$$\mathrm{uWFCP_b} = \frac{10 \times \sum_{t=1}^{\mathrm{gp}} \mathrm{ET_{b[t]}}}{Y} \quad (1)$$

$$\mathrm{uWFCP_g} = \frac{10 \times \sum_{t=1}^{\mathrm{gp}} \mathrm{ET_{g[t]}}}{Y} \quad (2)$$

where $\mathrm{uWFCP_b}$ and $\mathrm{uWFCP_g}$ are the blue and green uWFCP, respectively (m^3 ton^{-1}); $\mathrm{ET_b}$ and $\mathrm{ET_g}$ are the blue and green WFCP (that is, $\mathrm{WFCP_b}$ and $\mathrm{WFCP_g}$), respectively (mm) (see equations 8 and 9); gp represents the days in the growing period; 10 is the unit conversion factor; Y (see equation 4 below) is the crop yield (ton ha^{-1}); and t indicates a given day.

The daily aboveground biomass production (B) was obtained as follows:

$$B = \mathrm{WP^*} \times \sum \frac{\mathrm{Tr_{[t]}}}{\mathrm{ET_{0[t]}}} \quad (3)$$

where $\mathrm{WP^*}$ (ton ha^{-1}) expresses the aboveground dry matter produced per unit land area per unit of transpired water, which is governed by a combination of atmospheric CO_2 concentration, crop type (C3 and C4 crops), and soil fertility. The $\mathrm{WP^*}$ is multiplied with the ratio of crop transpiration (Tr) to the reference evapotranspiration ($\mathrm{ET_0}$) for that day. The goal of normalisation is to make $\mathrm{WP^*}$ applicable to diverse locations and seasons, including future climate scenarios.

The crop yield (Y) (ton ha^{-1}) was obtained by multiplying the aboveground biomass (B) with an adjusted reference harvest index:

$$Y = \mathrm{f_{HI}} \mathrm{HI_0} B \quad (4)$$

where $\mathrm{f_{HI}}$ is the calibration coefficient of the standardised harvest index $\mathrm{HI_0}$, which is influenced by water stress and temperature stress.

2.2.4 Dynamic daily soil water balance

By tracking the daily incoming and outgoing water fluxes at the root zone boundary, the dynamic daily soil water balance was calculated as follows (Mekonnen and Hoekstra, 2010):

$$S_{[t]} = S_{[t-1]} + \mathrm{PR_{[t]}} + \mathrm{IRR_{[t]}} + \mathrm{CR_{[t]}} - \mathrm{ET_{[t]}} - \mathrm{RO_{[t]}} - \mathrm{DP_{[t]}} \quad (5)$$

where S is the soil water content (mm); PR is the precipitation (mm); IRR is the irrigation water volume (mm); CR is the

capillary rise from groundwater, assumed to be zero (mm); RO is the surface runoff (mm); DP is the deep soil percolation (mm); and ET is the actual evapotranspiration (mm), consisting of soil evaporation (E) and crop transpiration (Tr), which were calculated as follows:

$$E = (\mathrm{K_r K_e})\mathrm{ET_0} \tag{6}$$

$$\mathrm{Tr} = \left(\mathrm{K_s K_{S_{Tr}} K_{C_{Tr}}}\right)\mathrm{ET_0} \tag{7}$$

where $\mathrm{K_r}$ is the evaporation reduction coefficient, which is less than 1 (dimensionless); $\mathrm{K_e}$ is the soil evaporation coefficient, which is proportional to the fraction of the soil surface not covered by the canopy (dimensionless); $\mathrm{K_s}$ is the soil water stress coefficient, which is smaller than 1 when there is insufficient soil water to meet the evaporative demand of the atmosphere (dimensionless); $\mathrm{K_{S_{Tr}}}$ is the cold stress coefficient, which drops below 1 when the temperature is insufficient for growth (dimensionless); and $\mathrm{K_{C_{Tr}}}$ is the crop transpiration coefficient, which is proportional to the green canopy cover (dimensionless).

By tracking the proportional contribution of daily rainfall and irrigation water to each element of the soil water balance, $\mathrm{ET_{b[}}_{t]}$, $\mathrm{ET_{g[}}_{t]}$, $E_{\mathrm{b}[t]}$, $E_{\mathrm{g}[t]}$, $\mathrm{Tr_{b[}}_{t]}$ and $\mathrm{Tr_{g[}}_{t]}$ were extracted (Zhuo et al., 2016c; Chukalla et al., 2015):

$$\mathrm{ET_{b}}[t] = \mathrm{IRR}_{[t]} + S_{\mathrm{b}[t-1]} - S_{\mathrm{b}[t]} - \mathrm{RO}_{[t]}\left(\frac{\mathrm{IRR}_{[t]}}{\mathrm{PR}_{[t]} + \mathrm{IRR}_{[t]}}\right) - \mathrm{DP}_{[t]}\left(\frac{S_{\mathrm{b}[t-1]}}{S_{[t-1]}}\right) \tag{8}$$

$$\mathrm{ET_{g}}[t] = \mathrm{PR}_{[t]} + S_{\mathrm{g}[t-1]} - S_{\mathrm{g}[t]} - \mathrm{RO}_{[t]}\left(\frac{\mathrm{PR}_{[t]}}{\mathrm{PR}_{[t]} + \mathrm{IRR}_{[t]}}\right) - \mathrm{DP}_{[t]}\left(\frac{S_{\mathrm{g}[t-1]}}{S_{[t-1]}}\right) \tag{9}$$

$$E_{\mathrm{b}[t]} = \mathrm{E}_{[t]}\left(\frac{S_{\mathrm{b}[t-1]}}{S_{[t-1]}}\right) \tag{10}$$

$$E_{\mathrm{g}[t]} = E_{[t]}\left(\frac{S_{\mathrm{g}[t-1]}}{S_{[t-1]}}\right) \tag{11}$$

$$\mathrm{Tr_{b}}[t] = \mathrm{Tr}_{[t]}\left(\frac{S_{\mathrm{b}[t-1]}}{S_{[t-1]}}\right) \tag{12}$$

$$\mathrm{Tr_{g}}[t] = \mathrm{Tr}_{[t]}\left(\frac{S_{\mathrm{g}[t-1]}}{S_{[t-1]}}\right) \tag{13}$$

where $\mathrm{S_{b[}}_{t]}$ and $\mathrm{S_{g[}}_{t]}$ are the blue and green soil water content (mm) for a crop, respectively, at the end of day t. Following Zhuo et al. (2016c), the green water value was used as the initial soil water content in each calculation cell.

2.2.5 Irrigation practices module

Different irrigation practices indirectly affect water consumption during the growth period due to differences in the fraction of the surface wetted (f_w) by each method (Raes et al., 2018). The soil evaporation coefficient ($\mathrm{K_e}$) was multiplied by the f_w-value to account for partial wetness when only a portion of any soil surface was irrigated. This irrigation practices differentiation approach is commonly used before (Pereira et al., 2015; Wang et al., 2019; Chibarabada et al., 2020; Li et al., 2022; Yue et al., 2022). We employed a supplementary irrigation strategy whereby irrigation is applied when soil moisture

falls below the plant wilting point to bring it up to field capacity. Owing to special environmental restrictions, furrow irrigation was used for rice planting in this study. Specific irrigation conditions were divided into either sufficient or water-demanding subtypes (irrigation to field capacity when the soil water content reached the wilting point).

$$K_e = f_w(1 - CC^*)K_{e_x} \quad (14)$$

$$(1 - CC^*) = 1 - 1.72CC + CC^2 - 0.3CC^3 \quad \geq 0 \quad (15)$$

where the f_w-values used for furrow, sprinkler, and micro-irrigation were 80%, 100%, and 40%, respectively; $(1 - CC^*)$ is the dimensionless adjusted fraction of the non-covered soil surface (dimensionless); CC is canopy cover (m^2 m^{-2}); and K_{e_x} is the maximum soil evaporation coefficient (dimensionless) for fully wet and non-shaded soil surfaces.

2.2.6 Benchmarks for uWFCP

In contrast to variables such as rain-fed and irrigated croplands, wet and dry years, warm and cold years, different soil types, climate zone was evidenced to be the key factor influencing regional uWFCP benchmarks (Zhuo et al., 2016b). Therefore, we classified China's climatic regions based on the aridity index (Middleton and Thomas, 1997) (AI; defined as the ratio of rainfall to reference evapotranspiration) and set up regional uWFCP benchmarks for humid (AI > 0.5) and arid (AI < 0.5) zones. The uWFCP of each grid in the same climate zone was ranked from lowest to highest, and the uWFCP corresponding to a cumulative crop production of 10%, 20% and 25% of the total production were recorded as the regional uWFCP benchmarks (Mekonnen and Hoekstra, 2014; Zhuo et al., 2016b; Wang et al., 2019; Yue et al., 2022).

2.3 Calibration and validation

2.3.1 Production calibration

Given the data accessibility, the current study utilized provincial statistics to validate the simulated production by scaling each grid-based simulated result using provincial calibration coefficients (R), rather than forcing the simulated production of all grid within a province to a constant value (Mialyk et al., 2022; Yue et al., 2022; Zhuo et al., 2016a). This approach maintained the spatial variability of simulated production within each province.

$$R = \frac{P\_P_{sta}}{\sum_{i=1}^{4} P\_G_{i,sim}} \quad (16)$$

$$P\_G_{i,act} = P\_G_{i,sim} \cdot R \quad (17)$$

where P_P_{NBSC} is the statistical (sta) provincial crop production (ton yr^{-1}); i represents the water supply modes and irrigation practices; $P\_G_{i,sim}$ is the simulated (sim) grid crop production value (ton yr^{-1}) according to i; and $P\_G_{i,act}$ is the actual (act) grid crop production value (ton yr^{-1}) according to i.

It should be noted that although provincial yearbooks include some city-level crop production data, considering the numerous crop types involved in this study, and the division of certain crops by harvest periods (e.g. winter wheat, spring wheat, early rice, mid rice, late rice), there are indeed many instances of missing and incomplete data at the city scale. The meteorological and soil factors are critical factors affecting the estimation of WFCP (Zhuo et al., 2014; Tuninetti et al., 2015). Consequently, the simulated outcomes can exhibit spatial heterogeneity after integrating high-resolution soil texture, precipitation, temperature, and other model inputs, even with provincial production calibration.

2.3.2 Remote sensing validation

Because of the spatially fragmented nature of crop cultivation, the water consumption results of current study were validated against the dual-source (PML-V2(China)) and single-source (SEBAL) remote sensing products over screened grids to reduce the interference of non-agricultural land with the validation results. According to Chinese Agricultural Cropping System (IGSNRR, 2022), we selected grids in which the sum of planted areas was greater than 5 kha (> 50% of a single grid) and greater than 10 kha (>100% of a single grid) for single- and multi-crop regions, respectively. In terms of the time span, 19 of the 21 crops studied experienced growth periods from April to August; therefore, these five months were set as the validation interval in terms of total evapotranspiration. The PML-V2 (He et al., 2022) and SEBAL (Cheng et al., 2021) products had spatial resolutions of 500 m and 1 km, respectively, with a temporal resolution of 1 day. Bilinear was implemented to resample the data to 5 arc-min. Notably, the SEBAL products solely comprised aggregate evapotranspiration figures, whereas the PML-V2 separated land surface evapotranspiration into vegetation transpiration (Ec), soil evaporation (Es), evaporation of intercepted precipitation (Ei), and water body evaporation (Ew). In this study, Ec + Es, Ec and Es were compared with the generated ET, E and T data, respectively.

2.3.3 Publications comparison

The present dataset was compared with published studies that included temporal and spatial data overlaps. The comparison included the crop planting area at the grid scale (IFPRI, 2019; Grogan et al., 2022), and the WFCP and uWFCP values at the grid and national scale (Mekonnen and Hoekstra, 2011; Zhuo et al., 2016a; Chiarelli et al., 2020; Cheng et al., 2021).

2.3.4 Accuracy assessment

The linear regression coefficient (R^2) was used to measure the consistency between the statistical data, remote sensing data, and simulated results. The Root Mean Square Error (*RMSE*) metric was utilized to evaluate model performance.

Mathematically, the R^2 and *RMSE* can be expressed as:

$$R^2 = \frac{(\sum_{i=1}^{n}(x_i - \bar{x}_i) \times (\mathrm{ref}_i - \overline{\mathrm{ref}}_i))^2}{\sum_{i=1}^{n}(x_i - \bar{x}_i)^2 \times \sum_{i=1}^{n}(\mathrm{ref}_i - \overline{\mathrm{ref}}_i)^2} \quad (18)$$

$$RMSE = \sqrt{\frac{1}{n}\sum_{i=1}^{n}(x_i - \mathrm{ref}_i)^2} \quad (19)$$

where n indicate the number of samples; x_i and ref_i represent the simulated and statistical values (remote sensing data), respectively; $\bar{x}_i$ and $\overline{\mathrm{ref}}_i$ are the mean values of the simulated and statistical values (remote sensing data), respectively.3 Results

3.1 Water footprint of crop production

During the study period, the WFCP of 21 crops in China increased by 13% to 690 Gm³ yr^{-1} in 2018, with $WFCP_b$ and $WFCP_g$ accounting for 29% and 71% of this increase, respectively. The $WFCP_b$ and $WFCP_g$ varied greatly across crops, time, and space. Table 3 presents the WFCP of the 21 crops under different water supply modes and irrigation practices in 2018. Maize (165 Gm³ yr^{-1}), rice (143 Gm³ yr^{-1}), and wheat (125 Gm³ yr^{-1}) had the highest annual average WFCP, accounting for 67% of the total WFCP. The WFCP of grapes (177%) and maize (94 Gm³ yr^{-1}) showed the greatest growth rate, with their planting areas expanding by 156% and 82%, respectively (NBSC, 2022).

Table 3. WFCP and planting area under different water supply modes and irrigation practices for 21 crops in 2018.

Crop	Furrow irrigation			Micro irrigation			Sprinkler irrigation			Rain–fed	
	$WFCP_b$ M m³ (△)	WFCPg M m³ (△)	Area k ha (△)	$WFCP_b$ M m³ (△)	WFCPg M m³ (△)	Area k ha (△)	$WFCP_b$ M m³ (△)	WFCPg M m³ (△)	Area k ha (△)	WFCPg M m³ (△)	Area k ha (△)
Wheat	40,595 (-22%)	35,702 (-9%)	13,157 (-18%)	4,384 (1936%)	2,369 (1650%)	1,357 (1964%)	2,170 (-26%)	1,583 (-10%)	625 (-20%)	41,046 (5%)	9,127 (-6%)
Maize	31,023 (3%)	40,092 (18%)	13,122 (12%)	5,581 (4577%)	3,604 (2950%)	1,611 (3413%)	4,351 (67%)	4,413 (107%)	1,538 (95%)	120,279 (162%)	25,859 (147%)
Rice	81,847 (4%)	58,979 (1%)	28,306 (-4%)	- -	- -	- -	4,629 (329%)	5,540 (404%)	1,883 (366%)	- -	- -
Sorghum	346 (-36%)	457 (-20%)	157 (-27%)	57 (3124%)	46 (2259%)	21 (2583%)	53 (34%)	53 (85%)	20 (66%)	1,757 (-35%)	424 (-36%)
Millet	346 (-27%)	388 (-10%)	137 (-20%)	43 (2176%)	32 (1786%)	16 (2032%)	46 (10%)	42 (41%)	16 (28%)	2,652 (-38%)	609 (-43%)
Barley	91 (-48%)	133 (-48%)	67 (-52%)	14 (4024%)	12 (3355%)	7 (2902%)	6 (-3%)	7 (3%)	3 (-13%)	768 (-67%)	235 (-65%)
Soybeans	3,936 (-22%)	6,751 (-16%)	1,963 (-19%)	413 (2315%)	375 (1871%)	144 (2031%)	389 (35%)	609 (102%)	193 (88%)	27,319 (-7%)	6,113 (-10%)
Potatoes	721 (-20%)	966 (11%)	377 (14%)	140 (3694%)	78 (2962%)	39 (3256%)	91 (50%)	88 (121%)	34 (106%)	16,171 (8%)	4,440 (1%)
Sweet potatoes	873 (-64%)	1,653 (-55%)	427 (-57%)	37 (429%)	57 (561%)	16 (513%)	37 (-67%)	59 (-44%)	16 (-51%)	10,276 (-60%)	1,921 (-60%)
Cotton	2,195 (-54%)	2,268 (-45%)	625 (-52%)	788 (4353%)	217 (1770%)	134 (3006%)	85 (-59%)	82 (-37%)	23 (-49%)	9,824 (-27%)	2,573 (-5%)
Sugar cane	258	589	98	9	20	3	8	17	3	10,924	1,302

	(-36%)	(-37%)	(-40%)	(1309%)	(1196%)	(1145%)	(163%)	(170%)	(150%)	(32%)	(28%)
Sugar beets	0.096	0.029	0.021	0.145	0.043	0.056	0.003	0.001	0.002	812	216
	(-78%)	(-78%)	(-72%)	(5530%)	(5859%)	(12331%)	(-85%)	(-85%)	(-61%)	(-34%)	(-34%)
Groundnuts	3,500	4,842	1,435	209	178	66	210	223	72	14,441	3,046
	(-6%)	(4%)	(-3%)	(1776%)	(1596%)	(1587%)	(11%)	(62%)	(42%)	(-6%)	(-8%)
Rapeseed	0.0159	0.0539	0.0147	0.0001	0.0002	0.0001	0.0001	0.0005	0.0001	19,053	6,551
	(256%)	(37%)	(67%)	(3336%)	(1653%)	(1800%)	(2660%)	(965%)	(1194%)	(3%)	(-13%)
Sunflower	262	202	87	137	49	33	34	21	10	2,913	792
	(-35%)	(-16%)	(-26%)	(8591%)	(5601%)	(6626%)	(-1%)	(22%)	(10%)	(-25%)	(-28%)
Tomatoes	1,365	1,581	949	74	57	44	74	69	47	-	-
	(48%)	(60%)	(45%)	(2379%)	(2463%)	(2270%)	(109%)	(198%)	(144%)	-	-
Apple	2,366	2,223	568	352	226	85	166	134	36	7,551	1,250
	(-47%)	(-32%)	(-41%)	(1638%)	(1236%)	(1452%)	(-53%)	(-37%)	(-44%)	(11%)	(2%)
Tea	2,218	3,200	550	51	86	15	68	92	16	13,803	1,730
	(65%)	(46%)	(43%)	(1690%)	(1622%)	(1464%)	(427%)	(453%)	(404%)	(242%)	(252%)
Tobacco	308	673	201	13	39	12	14	26	8	3,819	836
	(-30%)	(-12%)	(-18%)	(1181%)	(1800%)	(1848%)	(-34%)	(21%)	(4%)	(-28%)	(-29%)
Cabbage	1,523	2,642	897	72	96	42	76	124	45	-	-
	(-18%)	(-19%)	(-24%)	(1183%)	(1033%)	(1136%)	(15%)	(47%)	(28%)	-	-
Grapes	0.013	0.006	0.003	0.033	0.015	0.008	0.0004	0.0002	0.0001	3,869	725
	(-58%)	(-59%)	(-58%)	(17901%)	(17826%)	(18248%)	(-71%)	(-71%)	(-71%)	(177%)	(156%)

Note: "△" refers to the rate of change from 2000 to 2018. "-" indicates that no crops are grown.

In addition, the annual average proportions of WFCP attributable to furrow irrigation and rain-fed conditions reached 53% and 44%, respectively (Fig. S1). Nevertheless, the WFCP of sprinkler and micro-irrigation expanded by 11 and 19 $Gm^3\ yr^{-1}$, respectively, increasing their proportional contribution to the total WFCP by respective factors of 1.6 and 23. Over the same period, WFCP under furrow irrigation decreased by 5%. Considering the positive correlation between WFCP and the cultivated area under different water supply and irrigation practices, the above results reflect that sprinkler and micro-irrigation planting modes are being deployed more often on existing and freshly reclaimed farmland in China (NBSC, 2022). Given the large scale of crop cultivation in China, such a significant shift in irrigation practices will have important implications: (i) it will affect the quantification of national crop water consumption; (ii) it will create market opportunities while concurrently propelling technological innovation in the irrigation infrastructure. In conclusion, when quantifying and evaluating the WFCP, it is vital to consider the influence of various water supply modes and irrigation practices (Wang et al., 2019).

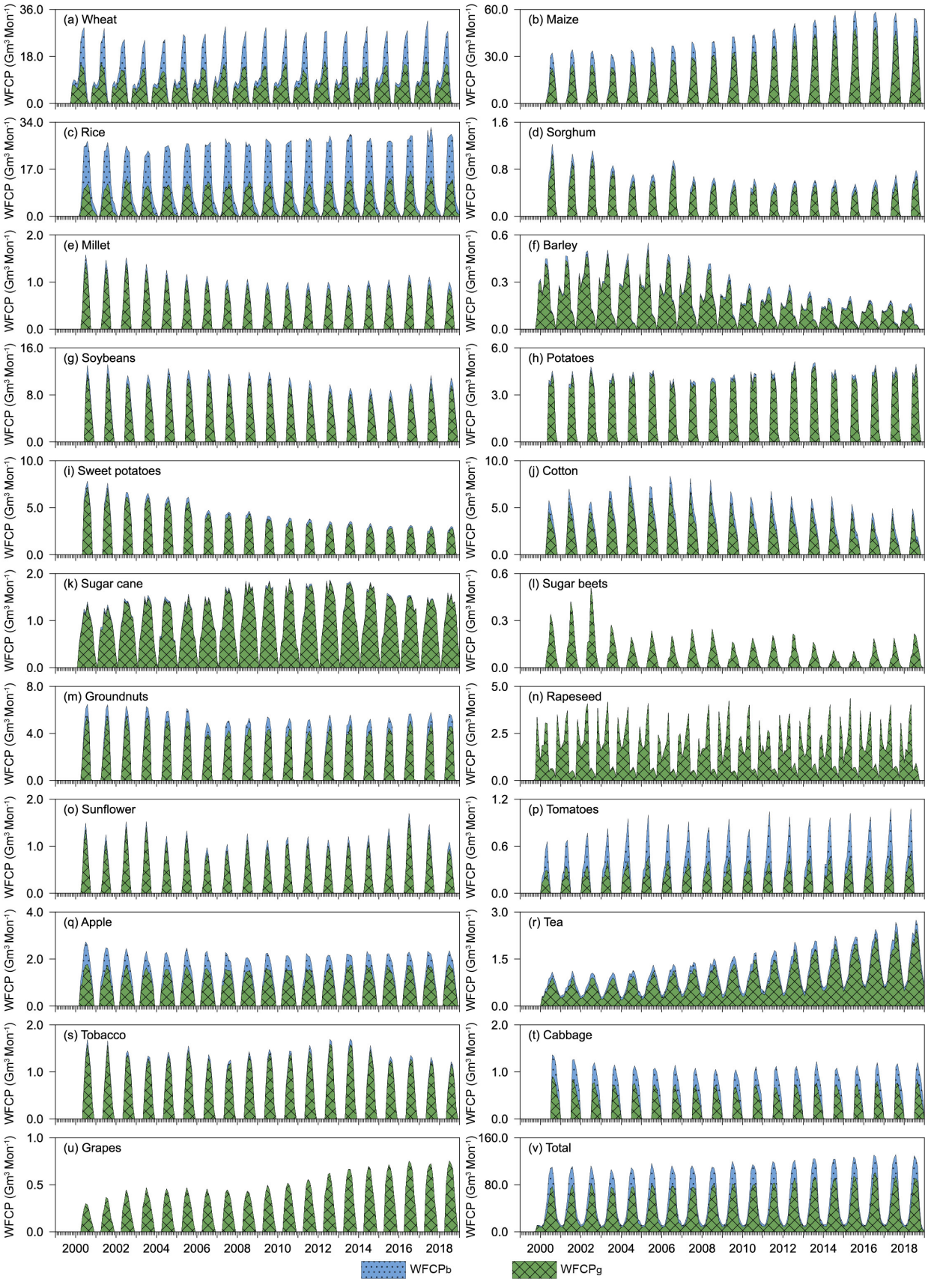

Figure 2. Total national monthly $WFCP_g$ and $WFCP_b$ of 21 crops in China over 2000-2018.

The water source accessed for crop production varied cyclically across years (Fig. 2). The $WFCP_b$ peaked annually in

May, with an average annual value of 16 $Gm^3\ mon^{-1}$; water usage by rice and maize crops were responsible for 40% and 37% of this value, respectively. In January and February of each year, the $WFCP_g$ comprised almost 75% of the monthly WFCP. The annual peak of the $WFCP_g$ alternated between June and July, with an average annual value of 83 $Gm^3\ mon^{-1}$, 40% of which was attributable to water consumption by maize crops. The monthly WFCP values revealed that the peaks of evaporation (average annual value of 45 $Gm^3\ mon^{-1}$) and transpiration (average annual value of 56 $Gm^3\ mon^{-1}$) for the 21 crops occurred in May and July, respectively (Fig. S2 and S3). The monthly WFCP fluctuated within each crop; nevertheless, the relative contributions of evapotranspiration and transpiration to total water consumption during the same growth period varied less from year to year. The above analysis allowed us to identify the quantity, type, and periods of water consumption by each crop.

The grid-scale spatial distributions of the monthly WFCP, $WFCP_b$, and $WFCP_g$ values are shown in Fig. 3. The months with large grid WFCP (WFCP > 50 mm mon^{-1}, $WFCP_b$ > 10 mm mon^{-1}, and $WFCP_g$ > 30 mm mon^{-1}) mainly comprised April to August. The Northeast Plain, North Plain, and Sichuan Basin contained the regions with the highest grid WFCP. The grid WFCP varied considerably among the 21 crops, but its spatial distribution was consistent within the planted area of each crop. In addition, the regional distribution of grid $WFCP_b$ and $WFCP_g$ values of each crop exhibited significant spatial heterogeneity (Fig. S4 and S5). The grid WFCP, $WFCP_b$, and $WFCP_g$ of sprinkler irrigation at the monthly and annual scales were significantly higher than those of the other two irrigation practices, and high-value regions were concentrated in the northeast, southwest, and south of China (Fig. S6–S10). This is attributable to the substantially higher surface wetting fraction achieved with sprinkler irrigation relative to furrow and micro irrigation, which augments crop water consumption per unit cultivated area during the growing period by affecting soil evaporation coefficient (Equations 6, 7 and 14). The relative blue and green water consumption via evaporation and transpiration depended on the natural conditions prevailing at the time and in the space where the 21 crops were grown, as well as the water supply modes and irrigation practices (Fig. S11–S14).

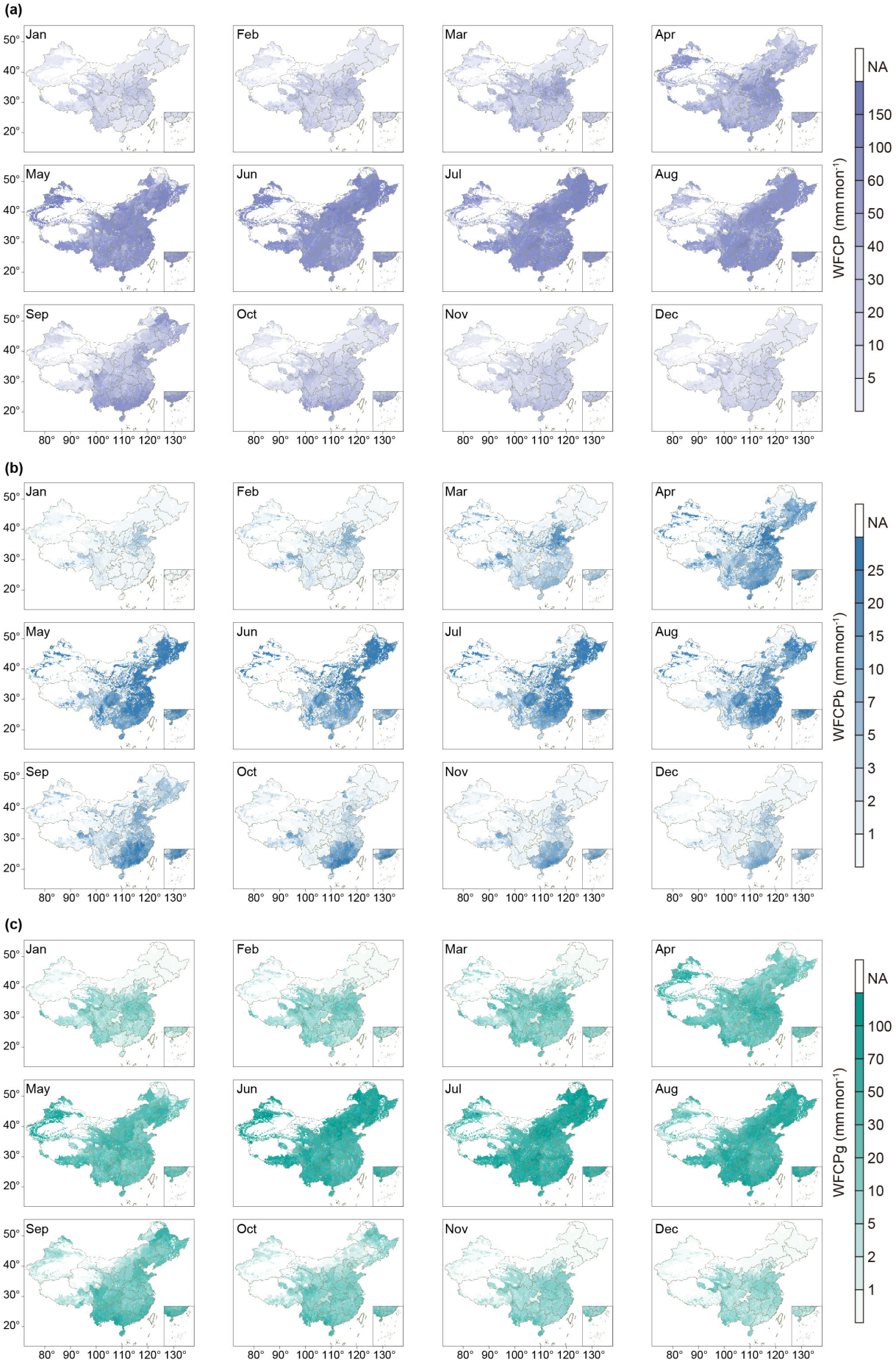

Figure 3. Gridded monthly total WFCP (a), WFCPb (b), and WFCPg (c) of 21crops in China by 2017.

3.2 Water footprint per unit of crop production

Tea (8372 m^3 ton^{-1}), cotton (3974 m^3 ton^{-1}), and tobacco (2242 m^3 ton^{-1}) had comparatively large uWFCP, whereas fruits and vegetables had a uWFCP of less than 500 m^3 ton^{-1}. Among the grain crops, wheat and maize had uWFCP of 1110 m^3 ton^{-1} and 883 m^3 ton^{-1}, respectively. Late rice (826 m^3 ton^{-1}) had a slightly greater uWFCP than early (654 m^3 ton^{-1}) and mid (732 m^3 ton^{-1}) rice. The uWFCP, $uWFCP_b$, and $uWFCP_g$ for all 21 crops showed a trend of fluctuating decline during the study period as yield grew (Fig. 4). The uWFCP of cotton (51%), sugar beets (52%), and apple (55%) showed the greatest reduction. The uWFCP of wheat and maize decreased by more than 25%, because the yield increased by 45% and 33%, respectively.

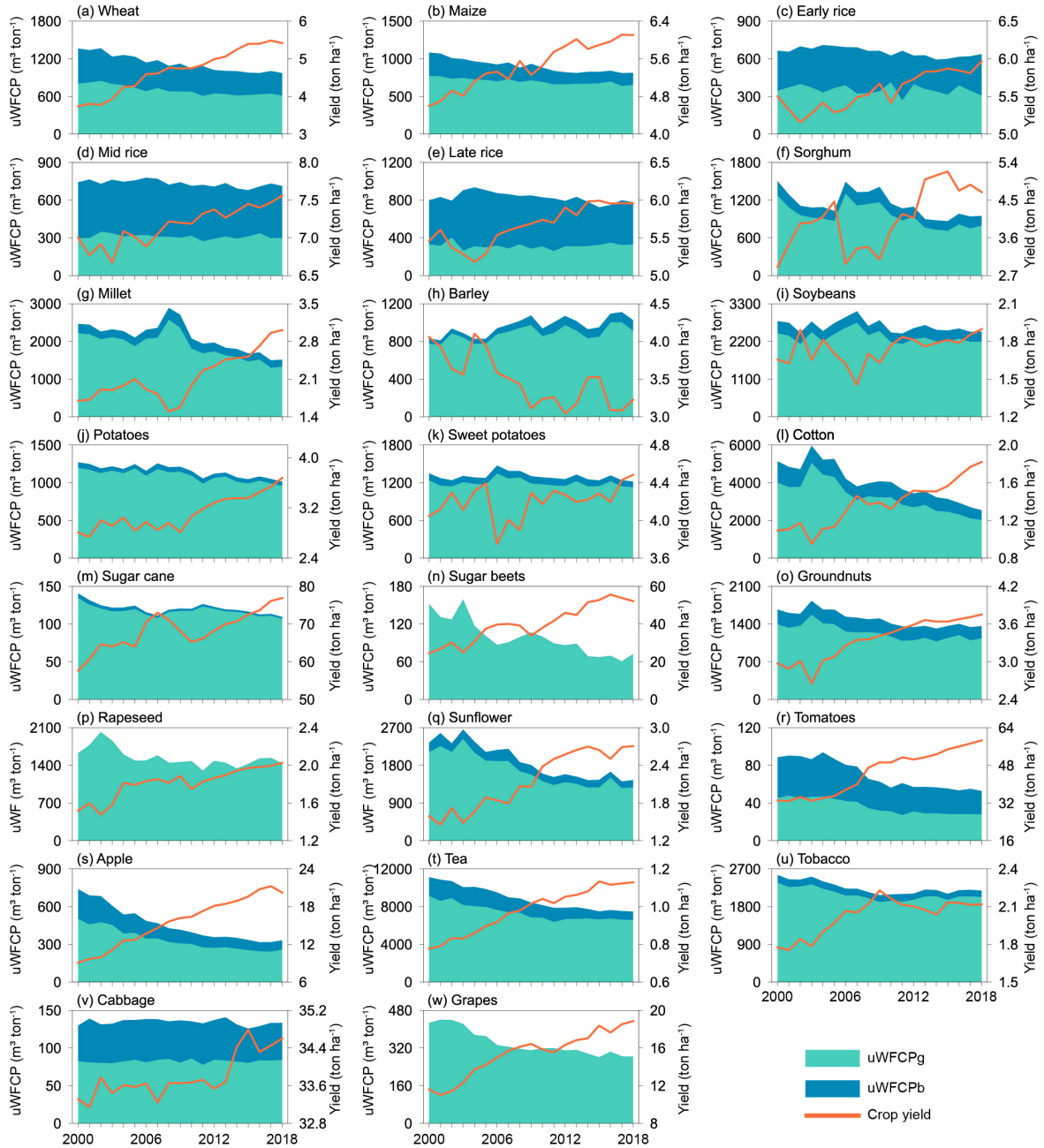

Figure 4. Interannual variation in uWFCPb, uWFCPg, and yield of 21crops in China over 2000-2018.

318 The uWFCP of the 21 crops was relatively high under rain-fed conditions (Table 4, Fig. S15). Additionally, the $uWFCP_b$,
319 $uWFCP_g$, and yield of each crop responded differently to the three irrigation treatments. These variations were caused by the
320 fact that the proportions of blue and green water consumption via soil evaporation and crop transpiration differed between
321 crops and irrigation practices (Fig. S16). For example, blue water consumption via crop transpiration in furrow and sprinkler
322 irrigation accounted for 45% and 51% of the total crop water consumption, respectively, which was much lower than that of
323 micro-irrigation (62%). Therefore, the effects of different water supply modes and irrigation practices should be considered in
324 the quantification of uWFCP over a long time series.
325
326 **Table 4. The uWFCPb, uWFCPg, and yield of 21crops under different water supply modes and irrigation practices in 2018.**

Crop	Furrow irrigation			Micro irrigation			Sprinkler irrigation			Rain–fed	
	Blue uWFCP m^3 ton^{-1} (△)	Green uWFCP m^3 ton^{-1} (△)	Yield ton ha^{-1} (△)	Blue uWFCP m^3 ton^{-1} (△)	Green uWFCP m^3 ton^{-1} (△)	Yield ton ha^{-1} (△)	Blue uWFCP m^3 ton^{-1} (△)	Green uWFCP m^3 ton^{-1} (△)	Yield ton ha^{-1} (△)	Green uWFCP m^3 ton^{-1} (△)	Yield ton ha^{-1} (△)
Wheat	508	447	6.1	628	340	5.1	636	464	5.5	999	4.5
	(-30%)	(-18%)	(36%)	(-18%)	(-29%)	(20%)	(-31%)	(-16%)	(35%)	(-38%)	(80%)
Maize	369	477	6.4	369	238	9.4	390	396	7.3	820	5.7
	(-26%)	(-15%)	(25%)	(-26%)	(-52%)	(80%)	(-38%)	(-24%)	(39%)	(-26%)	(43%)
Early rice	231	406	0.2	–	–	–	332	305	172.6	–	–
	(4%)	(-6%)	(463%)	–	–	–	(4%)	(-12%)	(-79%)	–	–
Mid rice	349	382	0.6	–	–	–	420	291	91.7	–	–
	(-24%)	(-4%)	(361%)	–	–	–	(-5%)	(-2%)	(-73%)	–	–
Late rice	237	540	0.2	–	–	–	454	322	156.6	–	–
	(8%)	(-2%)	(526%)	–	–	–	(-3%)	(-2%)	(-81%)	–	–
Sorghum	601	793	3.7	713	567	3.8	693	696	3.9	805	5.2
	(-43%)	(-29%)	(54%)	(-21%)	(-42%)	(52%)	(-56%)	(-39%)	(82%)	(-39%)	(67%)
Millet	719	807	3.5	705	531	3.8	712	652	4.0	1,528	2.8
	(-45%)	(-32%)	(65%)	(-36%)	(-47%)	(68%)	(-51%)	(-38%)	(76%)	(-38%)	(75%)
Barley	369	536	3.7	660	558	2.9	1,038	1,069	2.1	1,051	3.1
	(15%)	(15%)	(-7%)	(86%)	(55%)	(-26%)	(117%)	(130%)	(-48%)	(25%)	(-24%)
Soybeans	915	1,569	2.2	1,359	1,236	2.1	1,006	1,575	2.0	2,489	1.8
	(-14%)	(-8%)	(12%)	(-1%)	(-19%)	(14%)	(-29%)	(6%)	(2%)	(-11%)	(16%)
Potatoes	192	258	9.9	188	105	19.0	156	150	17.0	1,253	2.9
	(-10%)	(25%)	(-22%)	(-14%)	(-30%)	(31%)	(-3%)	(42%)	(-24%)	(-28%)	(47%)
Sweet potatoes	403	762	5.1	485	751	4.9	457	721	5.2	1,231	4.3
	(-26%)	(-7%)	(14%)	(-22%)	(-3%)	(11%)	(-38%)	(4%)	(9%)	(-8%)	(10%)
Cotton	2,539	2,623	1.4	1,306	360	4.5	2,807	2,704	1.3	2,133	1.8
	(-18%)	(-3%)	(17%)	(-53%)	(-80%)	(208%)	(-22%)	(20%)	(3%)	(-55%)	(71%)
Sugar cane	16	37	164.9	13	29	200.7	19	41	146.1	120	69.8
	(-31%)	(-32%)	(56%)	(-10%)	(-17%)	(26%)	(-43%)	(-41%)	(83%)	(-26%)	(40%)
Sugar beets	8	2	752.3	7	2	786.0	10	4	520.9	72	52.2
	(-35%)	(-36%)	(54%)	(-35%)	(-32%)	(49%)	(-26%)	(-23%)	(30%)	(-53%)	(114%)
Groundnuts	440	608	5.5	633	540	5.0	534	567	5.5	1,669	2.8
	(-35%)	(-29%)	(50%)	(0%)	(-10%)	(11%)	(-41%)	(-14%)	(32%)	(-5%)	(8%)
Rapeseed	181	611	6.0	116	676	6.0	181	611	6.0	1,435	2.0
	(35%)	(-48%)	(58%)	(19%)	(-39%)	(52%)	(35%)	(-48%)	(58%)	(-12%)	(34%)

Sunflower	829	639	3.6	694	250	6.0	794	485	4.5	1,504	2.4
	(-27%)	(-6%)	(21%)	(-42%)	(-62%)	(121%)	(-30%)	(-13%)	(28%)	(-39%)	(72%)
Tomatoes	25	28	58.6	28	22	58.7	27	25	58.6	–	–
	(-43%)	(-38%)	(77%)	(-41%)	(-39%)	(77%)	(-52%)	(-31%)	(77%)	–	–
Apple	159	150	26.1	200	128	20.9	219	177	21.1	345	17.5
	(-65%)	(-56%)	(159%)	(-40%)	(-54%)	(87%)	(-66%)	(-55%)	(151%)	(-48%)	(111%)
Tea	1,769	2,552	2.3	1,546	2,601	2.2	1,620	2,218	2.6	10,769	0.7
	(-52%)	(-57%)	(138%)	(-64%)	(-66%)	(221%)	(-65%)	(-63%)	(198%)	(-17%)	(17%)
Tobacco	596	1,303	2.6	486	1,436	2.2	622	1,110	2.9	2,281	2.0
	(-25%)	(-5%)	(13%)	(-24%)	(13%)	(-14%)	(-40%)	(9%)	(6%)	(-15%)	(20%)
Cabbage	49	85	34.7	53	71	32.7	48	79	35.0	–	–
	(4%)	(2%)	(4%)	(6%)	(-7%)	(-2%)	(-14%)	(9%)	(5%)	–	–
Grapes	135	63	33.8	115	54	33.8	148	64	33.8	283	18.8
	(-44%)	(-45%)	(80%)	(-45%)	(-46%)	(80%)	(-44%)	(-45%)	(80%)	(-34%)	(63%)

Note: "△" refers to the rate of change from 2000 to 2018. "-" indicates that no crops are grown.

The spatial distribution of the gridded uWFCP showed significantly heterogeneity (Fig. 5, S17, and S18). There were many regions with high-gridded uWFCP values for potatoes, which were concentrated in northern China. The crop with the densest distribution of high-gridded $uWFCP_b$ values was tea, which was commonly dispersed throughout the southern regions. Soybean and millet possessed more $uWFCP_g$ high-value areas, mainly in the northern regions. By comparing the relative changes in the average grid uWFCP from the period of 2000-2009 to that of 2010-2018, it was determined that the uWFCP of all 21 crops exhibited a spatially significant decreasing trend (Fig. S19–S21). It is essential to emphasise that the dominant factors governing this decrease in uWFCP varied among crops. For example, the decline observed in the uWFCP of apple was attributable to a substantially larger decrease in $uWFCP_g$ than the corresponding rise in $uWFCP_b$, whereas that observed for tea was caused by a considerable decrease in $uWFCP_b$.

For most crops, rainfed ones had more regions of high uWFCP than irrigated ones, and the geographical distribution of uWFCP for the same crop was generally consistent, regardless of irrigation practices. The variation in $uWFCP_b$ and $uWFCP_g$ for the same water supply mode and irrigation practice in a crop was considerable owing to regional water consumption and yield differences (Fig. S22 and S23). Additionally, the temporal evolution of $uWFCP_b$ and $uWFCP_g$ under various water supply modes and irrigation practices was analysed, and rainfed crops demonstrated a more rapid and wider reduction in uWFCP than irrigated crops.

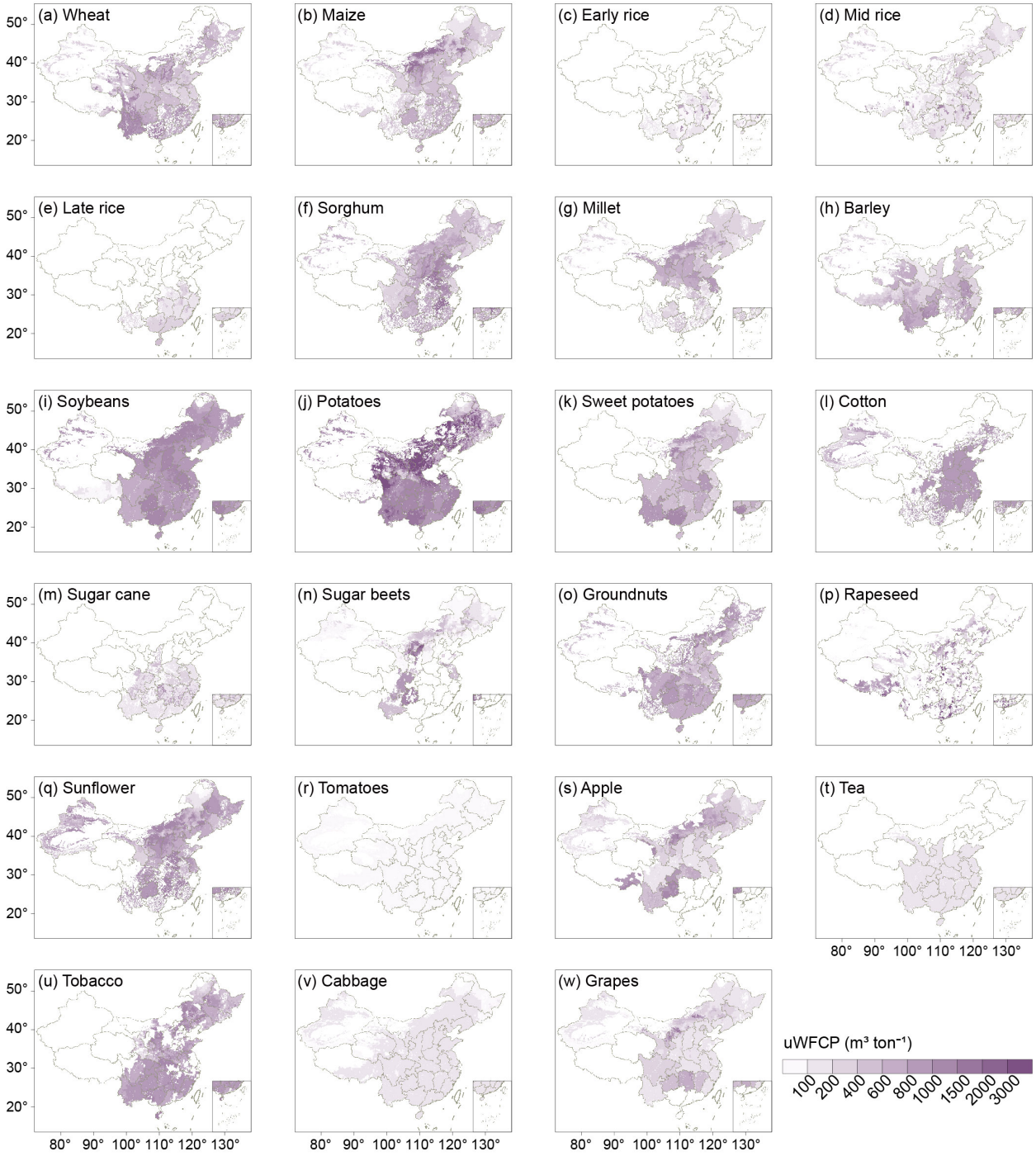

Figure 5. Gridded uWFCP of 21 crops in China at annual average level for 2000-2018.

3.3 Benchmarks for uWFCP

Annual uWFCP benchmarks were calculated using the different production percentiles for each of the 21 crops under various water supply modes and irrigation practices. Significant interannual differences existed between these uWFCP benchmarks, therefore, we reassessed these benchmarks using whole time series measurements to reduce the impact of anomalous values resulting from extreme climate events. The crops uWFCP benchmarks in Table S1 can be selected as a

reference for future analysis like Yue et al. (2022). Results show that benchmarks for the uWFCP of different crops responded differently to climatic zone. Crops such as millet, soybeans, and groundnuts had higher benchmarks for uWFCP in arid zones than in humid zones due to differences in production percentiles; the reverse was true for maize, cotton, and sunflower. Several factors contribute to these results. Firstly, crops cultivated in arid zones are more irrigation-reliant due to scarce precipitation and undergo greater evapotranspiration, resulting in higher uWFCP versus humid zones. Secondly, certain crops like cotton possess higher benchmarks in humid zones since their yields are markedly lower than those extensively grown in arid regions. Overall, the uWFCP benchmarks for rainfed crops were higher than those for irrigated crops. The uWFCP benchmarks for each irrigation practice varied by crop species.

Fig. 6 and Fig. S26–S28 present the uWFCP benchmarks according to different production percentiles in humid and arid zones and as obtained for various water supply modes and irrigation practices. Except for vegetables (tomatoes and cabbage), the majority of crops were cultivated in regions with a uWFCP benchmark that exceeded the 25% production percentile. Under furrow and sprinkler irrigation, the areas that fell below the uWFCP benchmark at the 25% production percentile were predominantly distributed in the humid zone. In the arid zone, a greater proportion of micro-irrigated regions fell below the uWFCP benchmark at the 25% production percentile. The results indicate that governing bodies need to consider the influence of climatic zones as well as water supply modes and irrigation practices when quantifying uWFCP benchmarks to identify hotspots for water-saving potential; specific water-use policies need to be formulated both for crop varieties and irrigation practices.

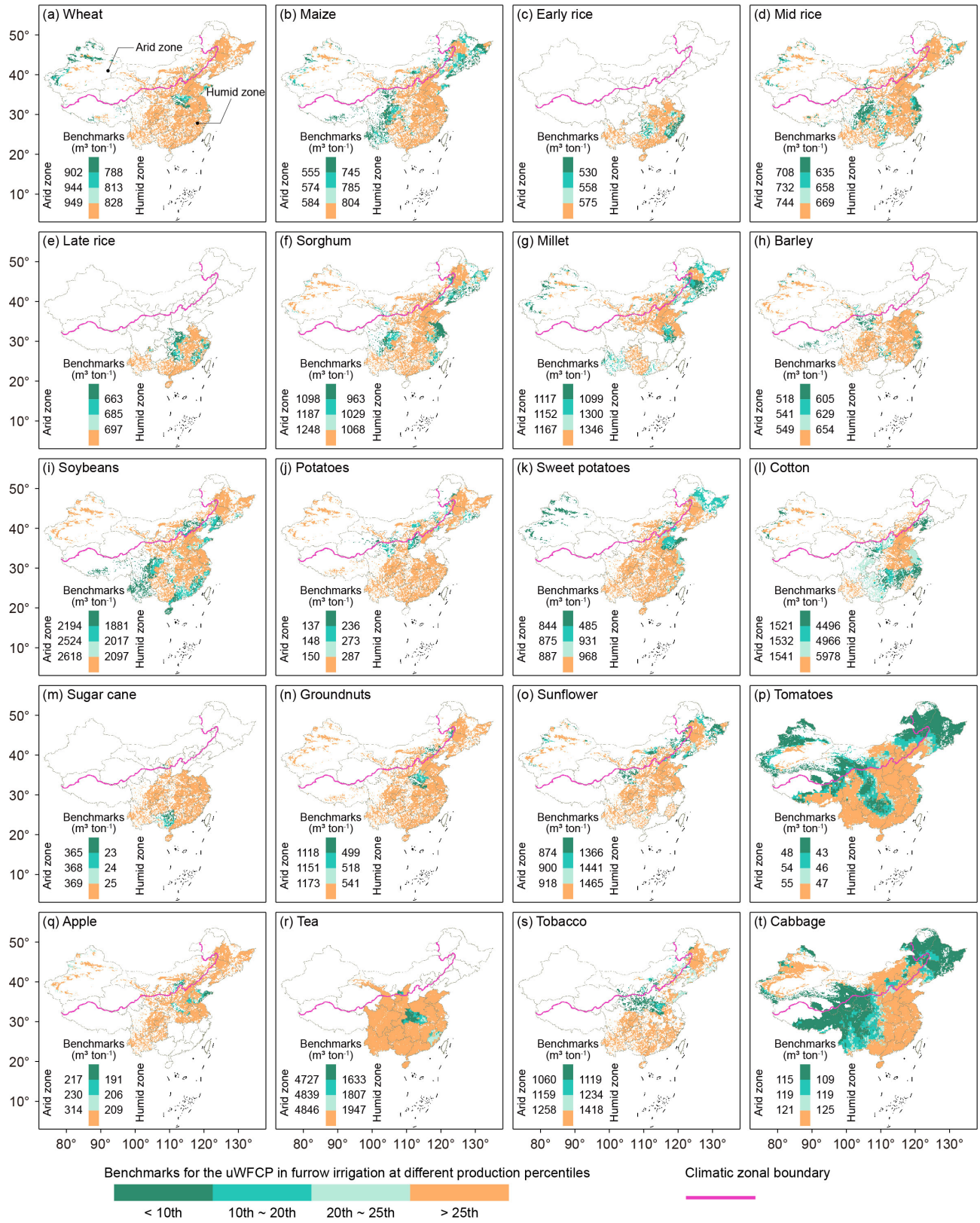

371

372 **Figure 6. Benchmarks for uWFCP at different production percentiles under furrow irrigation in China by 2018.**

373

3.4 Results comparison

Using publicly available datasets, we compared the water use of 15 crops with the WATNEEDS dataset (Chiarelli et al., 2020) that overlapped in time (in 2000) and space (137,956 grids). As illustrated in Fig. 7, the results showed that $R^2 > 0.60$ ($p < 0.01$) among 12 of the crops. However, large deviations were present in the comparisons of data for barley, sunflower, and potatoes. The following two factors were responsible for this disparity. First, the current study aimed to quantify the actual water consumption during crop growth, whereas the WATNEEDS dataset concentrated on theoretical crop water requirements. Second, this study divided irrigation into furrow, sprinkler, and micro-irrigation categories at the grid scale. In reality, sprinkler irrigation covers a much larger area than micro-irrigation does and also possesses the highest f_w of our three irrigation categories, which is ultimately reflected in a higher water consumption in our data. Overall, our dataset displayed a high level of reliability. The comparison of our WFCP data with the WATNEEDS dataset (Chiarelli et al., 2020) on a national scale is shown in Table 5. Except for rice, the variability of WFCP and $WFCP_b$ between the two datasets was under 25% and 20%, respectively, demonstrating high consistency. Large differences in the $WFCP_g$ between the two datasets can be attributed to two factors, namely, the different quantification methods used (including model mechanisms and green water definitions) and the different sources of precipitation data used for model input, leading to variations in green water simulations. With regards to the variability observed in rice data, some of our grids contained information for two to three seasons of rice cultivation (combined with the actual regional cultivation), and all these instances were assumed to receive irrigation in this study; this may have resulted in a comparatively low $WFCP_g$ value.

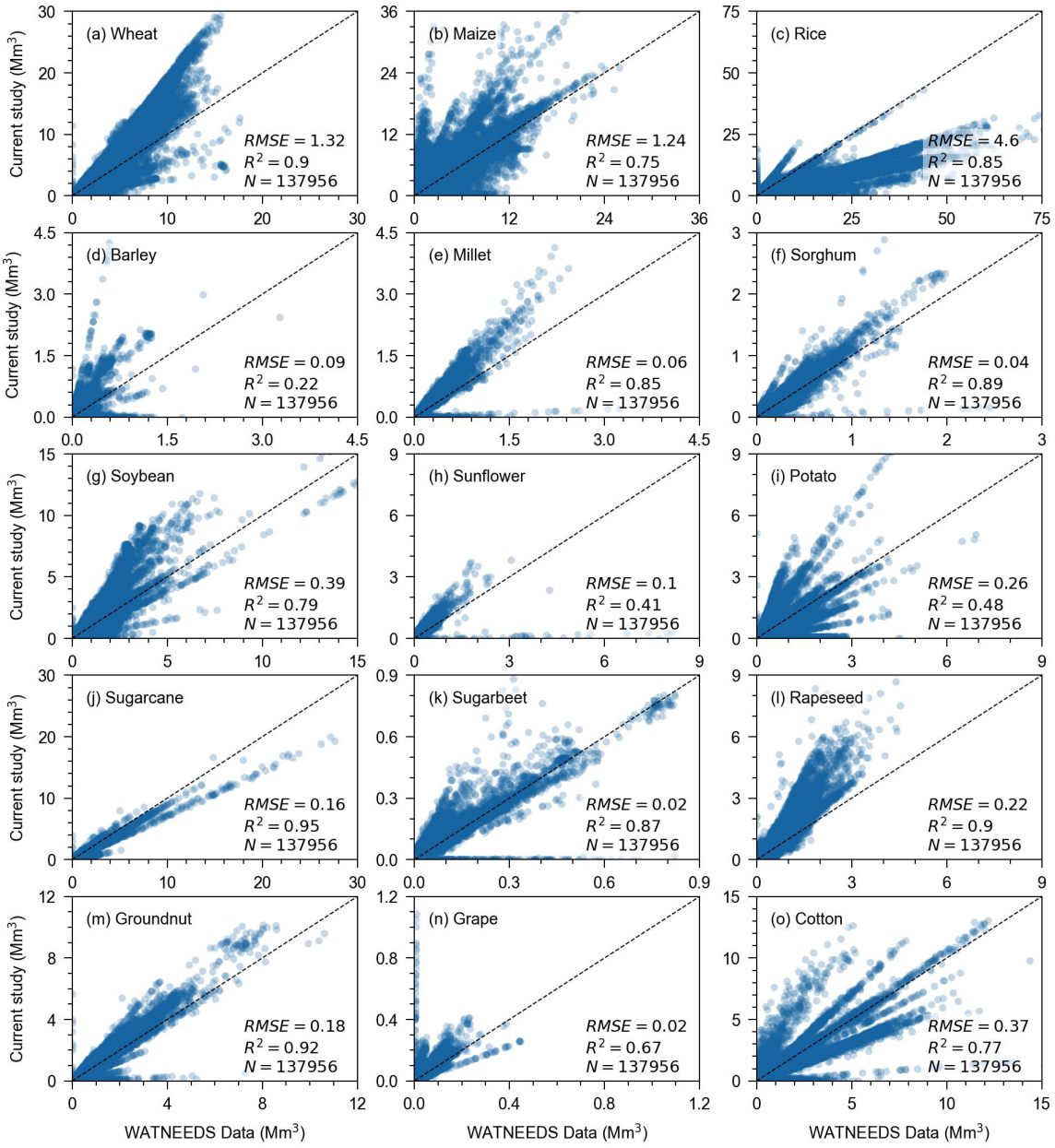

Figure 7. Comparison of WFCP with WATNEEDS dataset.

In a comparison of the uWFCP obtained for 21 crops in our dataset with figures reported by Mekonnen and Hoekstra (2011) and Zhuo et al. (2016a), the variability of data for 18 crops was under 30%, which was attributed to the uncertainty imposed by model simulation (Table 5). Although crop acreage remains consistent at the national scale, sets of crop distribution data must be matched with different sets of input variables (such as precipitation, temperature, and soil moisture content), which has a significant impact on the simulated values. The differences in the uWFCP of potato, sweet potato, and cotton resulted from the large discrepancies in production data, with simulated values for these three crops by Mekonnen and Hoekstra (2011) and Zhuo et al. (2016a) being 80%, 81%, and 67% higher than the statistical yearbook.

403 **Table 5. Comparison of WFCP and uWFCP in overlapping time and space with published results.**

Crop	WFCP Unit: M m^3 yr^{-1}. Period: 2000.					uWFCP Unit: m^3 ton^{-1}. Period: 2000-2005.					uWFCP Unit: m^3 ton^{-1}. Period: 2000-2009.				
	Current study		Chiarelli et al., 2020		(△)	Current study		Mekonnen and Hoekstra, 2011		(△)	Current study		Zhuo et al., 2016a		(△)
	Blue	Green	Blue	Green		Blue	Green	Blue	Green		Blue	Green	Blue	Green	
Wheat	80	55	79	22	(14%)	800	501	821	466	(1%)	754	472	1,135	392	(11%)
Maize	82	33	78	24	(6%)	744	264	791	74	(8%)	728	239	747	56	(9%)
Rice	59	80	255	97	(43%)	328	432	549	246	(2%)	323	437	987	395	(29%)
Sorghum	3	1	3	0	(4%)	1,002	178	952	42	(9%)	1,059	186	695	58	(25%)
Millet	5	1	4	0	(11%)	2,092	224	1,600	40	(17%)	2,145	242	1,418	141	(21%)
Barley	3	0	4	0	(21%)	804	50	556	28	(19%)	843	58	560	120	(14%)
Soybeans	38	5	33	5	(5%)	2,337	326	2,549	249	(2%)	2,418	317	2,336	316	(2%)
Potatoes	16	1	16	1	(0%)	1,163	62	215	7	(69%)	1,154	64	183	9	(73%)
Sweet potatoes	29	3				1,184	105	242	4	(68%)	1,211	108	63	22	(88%)
Cotton	18	5	23	3	(8%)	4,236	951	1,440	247	(51%)	3,781	847	1,117	281	(54%)
Sugar cane	9	0	12	1	(17%)	122	5	169	6	(16%)	118	4	124	1	(1%)
Sugar beets	1	0	1	0	(2%)	130	0	148	0	(6%)	117	0	104	0	(6%)
Groundnuts	20	4	19	3	(5%)	1,412	257	1,383	85	(6%)	1,347	260	1,399	219	(0%)
Rapeseed	18	0	12	0	(22%)	1,713	0	1,387	0	(11%)	1,623	0	1,754	0	(4%)
Sunflower	4	0	3	0	(9%)	2,154	232	2,254	341	(4%)	1,991	237	1,025	163	(30%)
Tomatoes	1	1				46	43	182	3	(35%)	42	39	81	2	(2%)
Apple	10	5				443	186	796	30	(14%)	389	154	372	46	(13%)
Tea	6	1				8,440	1,970	9,277	798	(2%)	7,860	1,792	9,055	122	(3%)
Tobacco	6	0				2,273	174	2,007	253	(4%)	2,162	167	1,771	18	(13%)
Cabbage	3	2				82	53	237	4	(28%)	82	53	122	8	(2%)
Grapes	1	0	1	0	(7%)	407	0	357	0	(7%)	364	0	349	123	(13%)

404 Note: "△" Calculated as the ratio of the study difference to the study mean.

405

406 **4 Discussion**

407 **4.1 Data validation**

408 We compared our 5 arcmin resolution of major crop areas, as calculated by the proportional invariant method, with the
409 GAEZ+ (Grogan et al., 2022) and SPAM (IFPRI, 2019) data products in the same year (Fig. 8). Linear regression results for
410 data on wheat, maize, and rice coverage showed that R^2 was greater than 0.50 ($p < 0.01$) at the raster scale and greater than
411 0.80 ($p < 0.01$) at the provincial scale, and the overall variability at the national scale was under 8%. We further compared

planting areas of other crops in SPAM and our data provincially and in grids (Fig. S29 and S30). It is evident that there is a high R^2 at the provincial scale. The differences at the grid scale can be attributed to discrepancies in the identification of gridded land use between the MIRCA2000 and SPAM. According to Fig. S31 and S32, the planting area data for sorghum, millet, barley, and sugar beets in the GAEZ+ exhibit significant deviations from this study, both at the provincial and grid scales. However, it should be emphasized that all crop planting area data in this study have been calibrated against statistical data at the provincial scale, implying an underestimation of the planting area for the mentioned crops in the GAEZ+. Overall, comparisons with existing products validated the accuracy of the gridded representation of crop land coverage as obtained in this study.

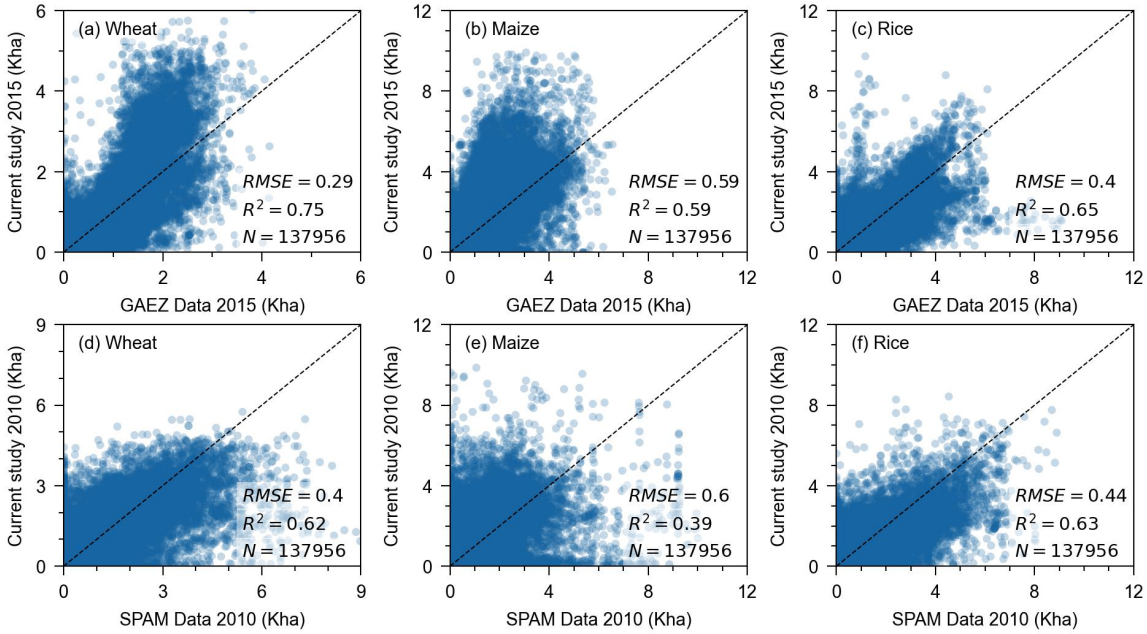

Figure 8. Comparison of the current gridded area representing land coverage by major crops with the GAEZ+ and SPAM datasets.

Based on data from dual-source (PML-V2(China)) and single-source (SEBAL) remote sensing products, we validated our evapotranspiration, evaporation and transpiration results specifically over the major cropping period from April to August by following the selection process outlined in Section 2.3.2. Comparative analysis in Fig.9 and Fig. S33 revealed stronger agreement between the simulated evapotranspiration and the PML-V2 products (R^2=0.49 – 0.85, *RMSE* =5.82 – 12.12 Mm^3) than those with the SEBAL products (R^2= 0.44 – 0.75, *RMSE* =8.51 – 15.82 Mm^3), although both comparisons demonstrated robust overall consistency. The validation results of soil evaporation (*E*) are presented in Fig. S34. The simulated *E* were marginally lower than the PML-V2 products (R^2=0.22 – 0.70, *RMSE* =3.25 – 6.65 Mm^3), owing to the current study calculating *E* exclusively for the planted regions of 21 crops, whereas the PML-V2 disregarded land use types during *E* estimation.

Comparative analysis of crop transpiration in Fig. S35 indicated that our simulated values were higher than the PML-V2 products which deducted canopy evaporation (R^2=0.38 – 0.69, *RMSE* =6.04 – 10.35 Mm^3). Overall, considering the differences in basic input data, spatiotemporal resolution and calculation methods, the evapotranspiration, evaporation, and transpiration data products produced in this study showed acceptable results when compared with various remote sensing products, given the discrepancies exhibited.

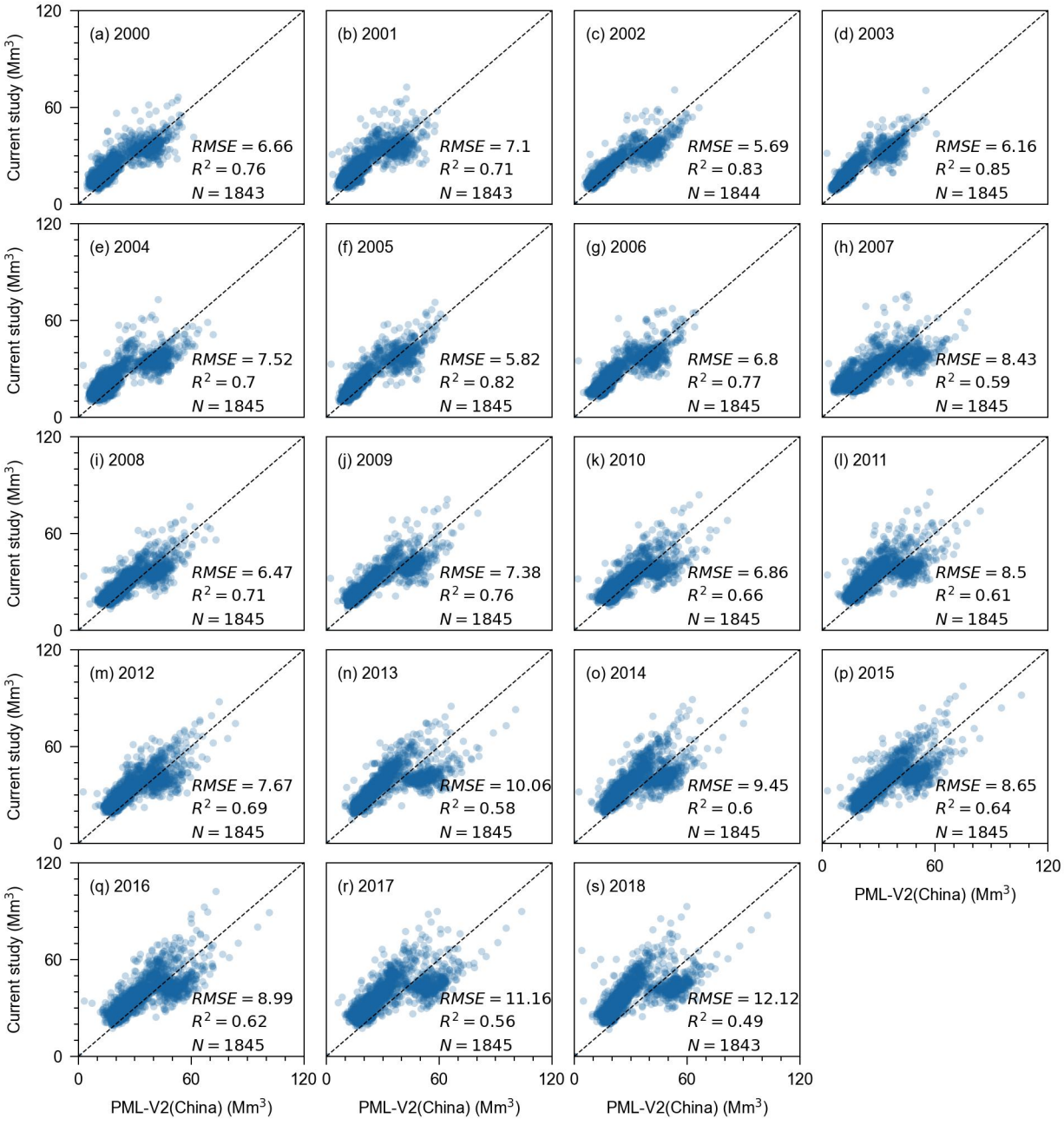

Figure 9. Validation of the evapotranspiration at croplands for the period April to August with PML-V2(China) datasets.

441 **4.2 Sensitivity and uncertainty analysis**

442 To clarify the sensitivity of a WFCP assessment to the main parameters in a simulation, a previous study by the authors
443 applied the one-at-a-time and sensitivity index methods to quantitatively evaluate a WFCP calculation by AquaCrop (Li et al.,
444 2022). The results indicated that crop water consumption and production were extremely sensitive to the reference
445 evapotranspiration, planting date (PD) and the crop transpiration coefficient (KcTr). The effect of PD differed for each crop,
446 and advancing or delaying it exposed crops to completely different rain and heat conditions. Minor shifts in PD forward or
447 backward have relatively small influences on WFCP since crop water consumption is primarily concentrated in crop
448 development and mid-season stages (Table S4 and Fig. S36). Moreover, yield and WFCP exhibited minimal sensitivity to
449 changes in crop PD when preserving constant growing degree days (Zhuo et al., 2014). In the Annex of the Reference manual
450 for the AquaCrop (Raes et al., 2018), default values of crop parameters for the crops covered in this study are given, including
451 crop transpiration, biomass production and yield formation, and stresses, totalling 41 parameters. Furthermore, these
452 parameters are further classified based on crop sensitivity as conservative generally applicable (including KcTr), conservative
453 for a given species but can or may be cultivar specific, dependent on environment and/or management and cultivar specific.
454 The conservative parameters are generally applicable and remain unchanged across a wide spectrum of conditions, including
455 different climatic and geographic locations, crop cultivars and genotypes, as well as variable soil moisture stress statuses. Once
456 calibrated, these identical parameters would be utilized without further modification. Importantly, the accuracy of all model
457 studies (including those using AquaCrop) is dependent on both the model mechanism and the input data. AquaCrop's accuracy
458 in simulating crop water consumption and production for various climates, soils, and field management practices has been
459 extensively validated (Zhuo et al., 2016a; Pirmoradian and Davatgar, 2019; Wang et al., 2019; Chibarabada et al., 2020).

460 At the outset of the simulation used in this study, we rigorously screened the input data according to the principles of
461 accuracy and representativeness. However, there was a degree of bias in the model setup and input data. For instance, the
462 current study focused on the effect of water stress on crop growth and worked from the assumption that all nutrients required
463 for crops were provided. Firstly, AquaCrop, as a water-driven model, simulates crop growth comprehensively by establishing
464 the responsive link between effective soil water usage and crop yield (Raes et al., 2018). Secondly, AquaCrop adopts a semi-
465 quantitative method to evaluate fertilizer stress. That is, it cannot directly simulate crop response to fertilizer based on plant
466 nutritional demand and soil nutrient content (Akumaga et al., 2017). Research shows AquaCrop performs better without
467 fertilizer stress versus with stress (Adeboye et al., 2021; Wu et al., 2022). In fact, there is a serious overapplication of chemical
468 fertilisers in Chinese farmlands (Chen et al., 2014; Cui and Shoemaker, 2018). The impact of fertilization on crop production
469 was indirectly reflected through calibration against statistical data. Thirdly, gridded data is deficient regarding fertilizer

varieties and application quantities, more so for crop-specific data. So like past AquaCrop global (Mialyk et al., 2022) and national (Wang et al., 2019) studies, nutrient stress is not considered in simulations. Certainly, the above assumption has limitations. Establishing high resolution fertilizer application databases is vital for future crop production research.

Furthermore, the parameters we used for fraction of the surface wetted in either furrow, sprinkler, or micro-irrigation remained consistent across regions owing to the absence of any data related to possible variance as mentioned in section 2.2.5; in other words, we downplayed regional variations within the same irrigation practice. Taking micro-irrigation as an example, the difference between different micro-irrigation products mostly lies in the transport and distribution pipe networks and irrigator, which have little impact on the fraction of the surface wetted in the crop root zone. In terms of crop parameters, strict regional differences were considered during the initial screening of the 21 crops' parameters. According to the regional classification results in Table S3, these key parameters like plant dating, reference harvest index, crop growth stages, and maximum root depth for this study are obtained by referring to the literatures described in section 2.1.3. These data have been validated to be reliable and applicable in large-scale studies (Cao et al., 2014; Zhuo et al., 2016a; Wang et al., 2019). Due to data limitations, the remaining parameters such as maximum canopy cover, canopy cover decline coefficient, canopy growth coefficient were assigned the mean values within the reference range provided in the Annex of the Reference manual for the AquaCrop. Although this approach may overlook certain potential variations, the use of mean values generally captures the central tendency of the data.

Unlike small-scale studies at site level that emphasize region-specific measured parameters for model simulation, large regional-scale studies often adopt literature-recommended parameter values during data collection, with greater focus on regional variability and wide adaptability of the parameters. (Hoekstra and Wiedmann 2014; Davis et al., 2017; Mekonnen and Hoekstra 2020; Lutz et al., 2022; Halpern et al., 2022; Liu et al., 2022; Chiarelli et al., 2022; Demay et al., 2023). It was neither practical nor feasible to calibrate crop parameters individually for each grid given the constraints of available data. Nevertheless, we have made every effort to ensure the reliability of the model input parameters within the existing limitations. Consequently, in future research, attention to the collection and organisation of basic data can play a positive role in the improvement of the model mechanism and accuracy of the output (Mekonnen and Hoekstra, 2010; Mekonnen and Hoekstra, 2011).

In general, despite the uncertainties in the input data, the calculated WFCP and uWFCP were in good agreement with existing studies at both the grid and national scales, and the dataset in the long time series was compatible with remote sensing products. The above analysis demonstrated that the findings of our current study correctly reflected water consumption during the crop growth period under various water supply modes and irrigation practices.

5 Data availability

All data used in this study are freely available with the links given in Sect. 2. The dataset presented in this article are available from the Zenodo repository at https://doi.org/10.5281/zenodo.7756013 (Wang et al., 2023). Both gridded consumptive water footprints, evaporation, transpiration, and associate benchmarks of crop production are provided.

6 Conclusions

The current study constructed a gridded WFCP database for 21 crops in China for 2000-2018 to reflect different water supply modes and irrigation practices, thereby addressing monthly blue and green water consumption in soil evaporation and crop transpiration. Additionally, we established uWFCP benchmarks for various climatic zones, water supply modes and irrigation practices. The current dataset was thoroughly validated. The results highlighted the necessity to explore the influences of different field management practices on WFCP quantification and benchmarking in future research.

The WFCP is a crucial indicator used for evaluating water consumption by crops and a key component to solving the problems associated with the environmental "footprint family" and "planetary boundary" (Galli et al., 2012; Hoekstra and Wiedmann, 2014; Steffen et al., 2015). The current dataset is able to support for precise crop water productivity assessments, agricultural water-saving evaluations, the development of sustainable irrigation techniques, cropping structure optimisation, and crop-related interregional virtual water trade analysis. The dataset can furthermore be applied to develop dynamic water management policies by virtue of its analysis of the spatial and temporal fluctuations in crop water consumption. The methodological framework for batch quantification of the WFCP can facilitate the updating of relative dataset and scale conversion studies.

Author contributions

LZ and PW designed the research. WW collected basic data, performed simulations, and conducted results validation and calibration. XJ conducted the sensitivity analysis. ZY, ZL, ML, HZ, RG, CY, and PZ performed simulations. WW and LZ wrote the original manuscript. LZ and PW revised the manuscript.

Competing interests

The contact author has declared that neither they nor their co-authors have any competing interests.

Acknowledgements

We thank all colleagues for their support and work. The dataset could not be established without the contributions of all participants.

Financial support

The study is financially supported by the Program for Cultivating Outstanding Talents on Agriculture, Ministry of Agriculture and Rural Affairs, People's Republic of China (13210321), the National Youth Talents Plan, and Chinese Universities Scientific Fund (2452021168) to LZ.

References

Adeboye, O. B., Schultz, B., Adeboye, A. P., Adekalu, K. O., and Osunbitan, J. A.: Application of the AquaCrop model in decision support for optimization of nitrogen fertilizer and water productivity of soybeans, Inf. Process, 8(3), 419-436, https://doi.org/10.1016/j.inpa.2020.10.002, 2021.

Akumaga, U., Tarhule, A., and Yusuf, A. A.: Validation and testing of the FAO AquaCrop model under different levels of nitrogen fertilizer on rainfed maize in Nigeria, West Africa, Agr. Forest Meteorol., 232, 225-234, https://doi.org/10.1016/j.agrformet.2016.08.011, 2017.

Allen, R. G., Pereira, L. S., Raes, D., and Smith, M.: Crop evapotranspiration—Guidelines for computing crop water requirements-FAO Irrigation and drainage paper 56, 300, D05109, FAO, Rome, 1998.

Batjes, N. H.: ISRIC-WISE derived soil properties on a 5 by 5 arc-minutes global grid (ver. 1.2), ISRIC-World Soil Information, available at: https://data.isric.org/geonetwork/srv/eng/catalog.search#/metadata/82f3d6b0-a045-4fe2-b960-6d05bc1f37c0. (last access: 7 March 2023), 2012.

Brown, J. F. and Pervez, M. S.: Merging remote sensing data and national agricultural statistics to model change in irrigated agriculture, Agric. Syst., 127, 28-40, https://doi.org/10.1016/j.agsy.2014.01.004, 2014.

Cao, X., Wu, P., Wang, Y., and Zhao, X.: Assessing blue and green water utilisation in wheat production of China from the perspectives of water footprint and total water use, Hydrol. Earth Syst. Sci., 18(8), 3165-3178, https://doi.org/10.5194/hess-18-3165-2014, 2014.

Chen, X., Cui, Z., Fan, M., Vitousek, P., Zhao, M., Ma, W., Wang, Z., Zhang, W., Yan, X., and Yang, J.: Producing more grain with lower environmental costs, Nature, 514, 486-489, https://doi.org/10.1038/nature13609, 2014.

549 Chen, Y., Guo, G., Wang, G., Kang, S., Luo, H., and Zhang, D.: Main crop water requirement and irrigation of China, Hydraulic
550 and Electric Press, Beijing, 1995.
551 Cheng, M., Jiao, X., Li, B., Yu, X., Shao, M., and Jin, X.: Long time series of daily evapotranspiration in China based on the
552 SEBAL model and multisource images and validation, Earth Syst. Sci. Data, 13, 3995-4017, https://doi.org/10.5194/essd-
553 13-3995-2021, 2021.
554 Chiarelli, D. D., Passera, C., Rosa, L., Davis, K. F., D'Odorico, P., and Rulli, M. C.: The green and blue crop water requirement
555 WATNEEDS model and its global gridded outputs, Sci. Data, 7, 273, https://doi.org/10.1038/s41597-020-00612-0, 2020.
556 Chiarelli, D. D., D'Odorico, P., Müller, M. F., Mueller, N. D., Davis, K. F., Dell'Angelo, J., Penny, G., and Rulli, M. C.:
557 Competition for water induced by transnational land acquisitions for agriculture, Nat. Commun., 13(1), 505,
558 https://doi.org/10.1038/s41467-022-28077-2, 2022.
559 Chibarabada, T., Modi, A., and Mabhaudhi, T.: Calibration and evaluation of aquacrop for groundnut (Arachis hypogaea) under
560 water deficit conditions, Agric. For. Meteorol., 281, 107850, https://doi.org/10.1016/j.agrformet.2019.107850, 2020.
561 CAMIYC, China Agricultural Machinery Industry Yearbook Committee: China Agricultural Machinery Industry Yearbook,
562 China Machine Press, Beijing, 2022.
563 Chukalla, A. D., Krol, M. S., and Hoekstra, A. Y.: Green and blue water footprint reduction in irrigated agriculture: effect of
564 irrigation techniques, irrigation strategies and mulching, Hydrol. Earth Syst. Sci., 19, 4877-4891,
565 https://doi.org/10.5194/hess-19-4877-2015, 2015.
566 Cui, K. and Shoemaker, S. P.: A look at food security in China, NPJ Sci. Food., 2, 4, https://doi.org/10.1038/s41538-018-0012-
567 x, 2018.
568 Davis, K. F., Rulli, M. C., Seveso, A., and D'Odorico, P.: Increased food production and reduced water use through optimized
569 crop distribution, Nat. Geosci., 10(12), 919-924, https://doi.org/10.1038/s41561-017-0004-5, 2017.
570 Demay, J., Ringeval, B., Pellerin, S., and Nesme, T.: Half of global agricultural soil phosphorus fertility derived from
571 anthropogenic sources, Nat. Geosci., 16(1), 69-74, https://doi.org/10.1038/s41561-022-01092-0, 2023.
572 Dijkshoorn, K., van Engelen, V., and Huting, J.: Soil and landform properties for LADA partner countries, ISRIC report,
573 available at: https://data.isric.org/geonetwork/srv/eng/catalog.search#/metadata/2919b1e3-6a79-4162-9d3a-
574 e640a1dc5aef. (last access: 7 March 2023), 2008.
575 Döll, P.: Vulnerability to the impact of climate change on renewable groundwater resources: a global-scale assessment, Environ.
576 Res. Lett., 4, 035006, https://doi.org/10.1088/1748-9326/4/3/035006, 2009.
577 Elliott, J., Deryng, D., Müller, C., Frieler, K., Konzmann, M., Gerten, D., Glotter, M., Flörke, M., Wada, Y., and Best, N.:
578 Constraints and potentials of future irrigation water availability on agricultural production under climate change, Proc.

Natl. Acad. Sci. U. S. A., 111, 3239-3244, https://doi.org/10.1073/pnas.1222474110, 2014.

FAO, Food and Agriculture Organization: The State of Food and Agriculture 2020. Overcoming water challenges in agriculture. Rome. https://doi.org/10.4060/cb1447en, 2020.

FAO, Food and Agriculture Organization: FAOSTAT statistical database, available at: https://www.fao.org/faostat/en/#data/QCL. (last access: 7 March 2023), 2023.

Fader, M., Gerten, D., Thammer, M., Heinke, J., Lotze-Campen, H., Lucht, W., and Cramer, W.: Internal and external green-blue agricultural water footprints of nations, and related water and land savings through trade, Hydrol. Earth Syst. Sci., 15, 1641-1660, https://doi.org/10.5194/hess-15-1641-2011, 2011.

Fisher, J. B., Melton, F., Middleton, E., Hain, C., Anderson, M., Allen, R., McCabe, M. F., Hook, S., Baldocchi, D., and Townsend, P. A.: The future of evapotranspiration: Global requirements for ecosystem functioning, carbon and climate feedbacks, agricultural management, and water resources, Water Resour. Res., 53, 2618-2626, https://doi.org/10.1002/2016WR020175, 2017.

Galli, A., Wiedmann, T., Ercin, E., Knoblauch, D., Ewing, B., and Giljum, S.: Integrating ecological, carbon and water footprint into a "footprint family" of indicators: definition and role in tracking human pressure on the planet, Ecol. Indic., 16, 100-112, https://doi.org/10.1016/j.ecolind.2011.06.017, 2012.

Ghose, B.: Food security and food self-sufficiency in China: from past to 2050, Food Energy Secur., 3, 86-95, https://doi.org/10.1002/fes3.48, 2014.

Grogan, D., Frolking, S., Wisser, D., Prusevich, A., and Glidden, S.: Global gridded crop harvested area, production, yield, and monthly physical area data circa 2015, Sci. Data, 9, 15, https://doi.org/10.1038/s41597-021-01115-2, 2022.

Haddeland, I., Heinke, J., Biemans, H., Eisner, S., Flörke, M., Hanasaki, N., Konzmann, M., Ludwig, F., Masaki, Y., and Schewe, J.: Global water resources affected by human interventions and climate change, Proc. Natl. Acad. Sci. U. S. A., 111, 3251-3256, https://doi.org/10.1073/pnas.1222475110, 2014.

Halpern, B. S., Frazier, M., Verstaen, J., Rayner, P.-E., Clawson, G., Blanchard, J. L., Cottrell, R. S., Froehlich, H. E., Gephart, J. A., Jacobsen, N. S., Kuempel, C. D., McIntyre, P. B., Metian, M., Moran, D., Nash, K. L., Többen, J., and Williams, D. R.: The environmental footprint of global food production, Nat. Sustain., 5(12), 1027-1039, https://doi.org/10.1038/s41893-022-00965-x, 2022.

Harris, I., Osborn, T. J., Jones, P., and Lister, D.: Version 4 of the CRU TS monthly high-resolution gridded multivariate climate dataset, Sci. Data, 7, 109, https://doi.org/10.1038/s41597-020-0453-3, 2020.

He, S., Zhang, Y., Ma, N., Tian, J., Kong, D., and Liu, C.: A daily and 500 m coupled evapotranspiration and gross primary production product across China during 2000–2020, Earth Syst. Sci. Data, 14, 5463-5488, https://doi.org/10.5194/essd-

609 14-5463-2022, 2022.
610 Hoekstra, A. Y.: The water footprint of modern consumer society, Routledge, London, 2013.
611 Hoekstra, A. Y. and Chapagain, A. K.: Water footprints of nations: water use by people as a function of their consumption
612 pattern, Water Resour. Manag., 21, 35-48, https://doi.org/10.1007/s11269-006-9039-x, 2006.
613 Hoekstra, A. Y. and Chapagain, A. K.: Globalization of water: Sharing the planet's freshwater resources, Blackwell Publishing,
614 Oxford, 2008.
615 Hoekstra, A. Y. and Wiedmann, T. O.: Humanity's unsustainable environmental footprint, Science, 344, 1114-1117,
616 https://doi.org/10.1126/science.1248365, 2014.
617 Hoekstra, A. Y., Chapagain, A. K., Aldaya, M. M., and Mekonnen, M. M.: The water footprint assessment manual: Setting the
618 global standard, Routledge, London, 2011.
619 Hoekstra, A.Y. and Mekonnen, M.M.: The water footprint of humanity. Proc. Natl. Acad. Sci. U. S. A., 109, 3232-3237,
620 https://doi.org/10.1073/pnas.1109936109, 2012.
621 Hoogeveen, J., Faurès, J.-M., Peiser, L., Burke, J., and van de Giesen, N.: GlobWat–a global water balance model to assess
622 water use in irrigated agriculture, Hydrol. Earth Syst. Sci., 19, 3829-3844, https://doi.org/10.5194/hess-19-3829-2015,
623 2015.
624 IFPRI, International Food Policy Research Institute: Global spatially-disaggregated crop production statistics data for 2010
625 version 2.0, available at: https://doi.org/10.7910/DVN/PRFF8V. (last access: 7 March 2023), 2019.
626 IGSNRR, Institute of Geographic Sciences and Natural Resources Research, CAS: Resource and Environment Science and
627 Data Center, available at: https://www.resdc.cn/data.aspx?DATAID=274. (last access: 7 March 2023), 2022.
628 Jägermeyr, J., Pastor, A., Biemans, H., and Gerten, D.: Reconciling irrigated food production with environmental flows for
629 Sustainable Development Goals implementation, Nat. Commun., 8, 15900, https://doi.org/10.1038/ncomms15900, 2017.
630 Jung, M., Reichstein, M., Ciais, P., Seneviratne, S. I., Sheffield, J., Goulden, M. L., Bonan, G., Cescatti, A., Chen, J., and De
631 Jeu, R.: Recent decline in the global land evapotranspiration trend due to limited moisture supply, Nature, 467, 951-954,
632 https://doi.org/10.1038/nature09396, 2010.
633 Leng, G., Huang, M., Tang, Q., Gao, H., and Leung, L. R.: Modeling the effects of groundwater-fed irrigation on terrestrial
634 hydrology over the conterminous United States, J. Hydrometeorol., 15, 957-972, https://doi.org/10.1175/JHM-D-13-
635 049.1, 2014.
636 Li, Z., Feng, B., Wang, W., Yang, X., Wu, P., and Zhuo, L.: Spatial and temporal sensitivity of water footprint assessment in
637 crop production to modelling inputs and parameters, Agric. Water Manage, 271, 107805,
638 https://doi.org/10.1016/j.agwat.2022.107805, 2022.

639 Lian, X., Piao, S., Huntingford, C., Li, Y., Zeng, Z., Wang, X., Ciais, P., McVicar, T. R., Peng, S., and Ottlé, C.: Partitioning
640 global land evapotranspiration using CMIP5 models constrained by observations, Nat. Clim. Chang., 8, 640-646,
641 https://doi.org/10.1038/s41558-018-0207-9, 2018.
642 Liu, J., Williams, J. R., Zehnder, A. J., and Yang, H.: GEPIC–modelling wheat yield and crop water productivity with high
643 resolution on a global scale, Agric. Syst., 94, 478-493, https://doi.org/10.1016/j.agsy.2006.11.019, 2007.
644 Liu, X., Liu, W., Tang, Q., Liu, B., Wada, Y., and Yang, H.: Global agricultural water scarcity assessment incorporating blue
645 and green water availability under future climate change, Earths Future, 10, e2021EF002567,
646 https://doi.org/10.1029/2021EF002567, 2022.
647 Long, D. and Singh, V. P.: Assessing the impact of end-member selection on the accuracy of satellite-based spatial variability
648 models for actual evapotranspiration estimation, Water Resour. Res., 49, 2601-2618, https://doi.org/10.1002/wrcr.20208,
649 2013.
650 Lovarelli, D., Bacenetti, J., and Fiala, M.: Water Footprint of crop productions: A review, Sci. Total Environ., 548, 236-251,
651 https://doi.org/10.1016/j.scitotenv.2016.01.022, 2016.
652 Lutz, A. F., Immerzeel, W. W., Siderius, C., Wijngaard, R. R., Nepal, S., Shrestha, A. B., Wester, P., and Biemans, H.: South
653 Asian agriculture increasingly dependent on meltwater and groundwater, Nat Clim Chang, 12(6), 566-573,
654 https://doi.org/10.1038/s41558-022-01355-z, 2022.
655 Mekonnen, M. M. and Hoekstra, A. Y.: A global and high-resolution assessment of the green, blue and grey water footprint of
656 wheat, Hydrol. Earth Syst. Sci., 14, 1259-1276, https://doi.org/10.5194/hess-14-1259-2010, 2010.
657 Mekonnen, M. M. and Hoekstra, A. Y.: The green, blue and grey water footprint of crops and derived crop products, Hydrol.
658 Earth Syst. Sci., 15, 1577-1600, https://doi.org/10.5194/hess-15-1577-2011, 2011.
659 Mekonnen, M. M. and Hoekstra, A. Y.: Water footprint benchmarks for crop production: A first global assessment, Ecol. Indic.,
660 46, 214-223, https://doi.org/10.1016/j.ecolind.2014.06.013, 2014.
661 Mekonnen, M. M., and Hoekstra, A. Y.: Blue water footprint linked to national consumption and international trade is
662 unsustainable, Nat. Food, 1(12), 792-800, https://doi.org/10.1038/s43016-020-00198-1, 2020.
663 Mialyk, O., Schyns, J. F., Booij, M. J., and Hogeboom, R. J.: Historical simulation of maize water footprints with a new global
664 gridded crop model ACEA, Hydrol. Earth Syst. Sci., 26, 923-940, https://doi.org/10.5194/hess-26-923-2022, 2022.
665 Middleton, N. and Thomas, D.: World atlas of desertification: Second Edition, Arnold, London, 1997.
666 NBSC, National Bureau of Statistics: China Statistical Yearbook, China Statistical Press, Beijing 2022.
667 Pastor, A., Palazzo, A., Havlik, P., Biemans, H., Wada, Y., Obersteiner, M., Kabat, P., and Ludwig, F.: The global nexus of
668 food–trade–water sustaining environmental flows by 2050, Nat. Sustain., 2, 499-507, https://doi.org/10.1038/s41893-

019-0287-1, 2019.

Pereira, L. S., Paredes, P., Rodrigues, G. C., and Neves, M.: Modeling malt barley water use and evapotranspiration partitioning in two contrasting rainfall years. Assessing AquaCrop and SIMDualKc models, Agric Water Manag, 159, 239-254, https://doi.org/10.1016/j.agwat.2015.06.006, 2015.

Pirmoradian, N. and Davatgar, N.: Simulating the effects of climatic fluctuations on rice irrigation water requirement using AquaCrop, Agric. Water Manage., 213, 97-106, https://doi.org/10.1016/j.agwat.2018.10.003, 2019.

Portmann, F. T., Siebert, S., and Döll, P.: MIRCA2000—Global monthly irrigated and rainfed crop areas around the year 2000: A new high-resolution data set for agricultural and hydrological modeling, Glob. Biogeochem. Cycle, 24, GB1011, https://doi.org/10.1029/2008GB003435, 2010.

Puy, A., Lo Piano, S., and Saltelli, A.: Current models underestimate future irrigated areas, Geophys. Res. Lett., 47, e2020GL087360, https://doi.org/10.1029/2020GL087360, 2020.

Puy, A., Borgonovo, E., Lo Piano, S., Levin, S. A., and Saltelli, A.: Irrigated areas drive irrigation water withdrawals, Nat. Commun., 12, 4525, https://doi.org/10.1038/s41467-021-24508-8, 2021.

Raes, D., Steduto, P., Hsiao, T., and Fereres, E.: Reference Manual, Chapter3, AquaCrop Model, Version 6.1, FAO, Rome, 2018.

Rodell, M., Velicogna, I., and Famiglietti, J. S.: Satellite-based estimates of groundwater depletion in India, Nature, 460, 999-1002, https://doi.org/10.1038/nature08238, 2009.

Rosa, L., Chiarelli, D. D., Rulli, M. C., Dell'Angelo, J., and D'Odorico, P.: Global agricultural economic water scarcity, Sci. Adv., 6, eaaz6031, https://doi.org/10.1126/sciadv.aaz6031, 2020.

Siebert, S. and Döll, P.: Quantifying blue and green virtual water contents in global crop production as well as potential production losses without irrigation, J. Hydrol., 384, 198-217, https://doi.org/10.1016/j.jhydrol.2009.07.031, 2010.

SCIO, State Council Information Office: White Paper: the Grain Issue in China, available at: http://www.scio.gov.cn/zfbps/ndhf/1996/Document/307978/307978.htm, (last access: 7 March 2023), 1996.

Steffen, W., Richardson, K., Rockström, J., Cornell, S. E., Fetzer, I., Bennett, E. M., Biggs, R., Carpenter, S. R., De Vries, W., and De Wit, C. A.: Planetary boundaries: Guiding human development on a changing planet, Science, 347, 1259855, https://doi.org/10.1126/science.1259855, 2015.

Tamea, S., Tuninetti, M., Soligno, I., and Laio, F.: Virtual water trade and water footprint of agricultural goods: the 1961–2016 CWASI database, Earth Syst. Sci. Data, 13, 2025-2051, https://doi.org/10.5194/essd-13-2025-2021, 2021.

Tans, P., and Keeling, R.: Mauna Loa CO2 monthly mean data, https://gml.noaa.gov/ccgg/trends/data.html.

Tilman, D., Balzer, C., Hill, J., and Befort, B. L.: Global food demand and the sustainable intensification of agriculture, Proc.

699 Natl. Acad. Sci. U. S. A., 108, 20260-20264, https://doi.org/10.1073/pnas.1116437108, 2011.
700 Tuninetti, M., Tamea, S., Laio, F., and Ridolfi, L.: A Fast Track approach to deal with the temporal dimension of crop water
701 footprint, Environ. Res. Lett., 12, 074010, https://doi.org/10.1088/1748-9326/aa6b09, 2017.
702 Tuninetti, M., Tamea, S., D'Odorico, P., Laio, F., and Ridolfi, L.: Global sensitivity of high-resolution estimates of crop water
703 footprint, Water Resour. Res., 51, 8257-8272, https://doi.org/10.1002/2015WR017148, 2015.
704 Vanuytrecht, E., Raes, D., Steduto, P., Hsiao, T. C., Fereres, E., Heng, L. K., Vila, M. G., and Moreno, P. M.: AquaCrop: FAO's
705 crop water productivity and yield response model, Environ. Modell. Softw., 62, 351-360,
706 https://doi.org/10.1016/j.envsoft.2014.08.005, 2014.
707 Wada, Y., Wisser, D., Eisner, S., Flörke, M., Gerten, D., Haddeland, I., Hanasaki, N., Masaki, Y., Portmann, F. T., and Stacke,
708 T.: Multimodel projections and uncertainties of irrigation water demand under climate change, Geophys. Res. Lett., 40,
709 4626-4632, https://doi.org/10.1002/grl.50686, 2013.
710 Waha, K., Van Bussel, L., Müller, C., and Bondeau, A.: Climate-driven simulation of global crop sowing dates, Glob. Ecol.
711 Biogeogr., 21, 247-259, https://doi.org/10.1111/j.1466-8238.2011.00678.x, 2012.
712 Water Footprint Network.: WaterStat–water footprint statistics, available at: https://waterfootprint.org/en/resources/waterstat/.
713 (last access: 7 March 2023), 2020.
714 Wang, W., Zhuo, L., Li, M., Liu, Y., and Wu, P.: The effect of development in water-saving irrigation techniques on spatial-
715 temporal variations in crop water footprint and benchmarking, J. Hydrol., 577, 123916,
716 https://doi.org/10.1016/j.jhydrol.2019.123916, 2019.
717 Wang, W., Zhuo, L., Ji, X., Yue, Z., Li, Z., Li, M., Zhang, H., Gao, R., Yan, C., Zhang, P., and Wu, P.: CWFETB-China: Gridded
718 dataset of consumptive water footprints, evaporation, transpiration, and associate benchmarks of crop production in China
719 (2000-2018), Zenodo [data set], https://doi.org/10.5281/zenodo.7756013, 2023.
720 Wang, X., Müller, C., Elliot, J., Mueller, N. D., Ciais, P., Jägermeyr, J., Gerber, J., Dumas, P., Wang, C., and Yang, H.: Global
721 irrigation contribution to wheat and maize yield, Nat. Commun., 12, 1235, https://doi.org/10.1038/s41467-021-21498-5,
722 2021.
723 Wu, H., Yue, Q., Guo, P., Xu, X., and Huang, X.: Improving the AquaCrop model to achieve direct simulation of
724 evapotranspiration under nitrogen stress and joint simulation-optimization of irrigation and fertilizer schedules, Agric.
725 Water Manag, 266, 107599, https://doi.org/10.1016/j.agwat.2022.107599, 2022.
726 Xie, G., Han, D., Wang, X., and Lü, R.: Harvest index and residue factor of cereal crops in China, Journal of China agricultural
727 university, 16, 1-8, 2011(in Chinese).
728 Yin, Y., Tang, Q., Liu, X., and Zhang, X.: Water scarcity under various socio-economic pathways and its potential effects on

food production in the Yellow River basin, Hydrol. Earth Syst. Sci., 21, 791-804, https://doi.org/10.5194/hess-21-791-2017, 2017.

Yue, Z., Ji, X., Zhuo, L., Wang, W., Li, Z., and Wu, P.: Spatiotemporal responses of the crop water footprint and its associated benchmarks under different irrigation regimes to climate change scenarios in China, Hydrol. Earth Syst. Sci., 26, 4637-4656, https://doi.org/10.5194/hess-26-4637-2022, 2022.

Zhang, F. and Zhu, Z.: Harvest index for various crops in China, Scientia Agricultura Sinica, 23, 83-87, 1990 (in Chinese).

Zhuo, L., Mekonnen, M. M., and Hoekstra, A. Y.: Sensitivity and uncertainty in crop water footprint accounting: a case study for the Yellow River basin, Hydrol. Earth Syst. Sci., 18(6), 2219-2234, https://doi.org/10.5194/hess-18-2219-2014, 2014.

Zhuo, L., Mekonnen, M. M., and Hoekstra, A. Y.: The effect of inter-annual variability of consumption, production, trade and climate on crop-related green and blue water footprints and inter-regional virtual water trade: A study for China (1978–2008), Water Res., 94, 73-85, https://doi.org/10.1016/j.watres.2016.02.037, 2016a.

Zhuo, L., Mekonnen, M. M., and Hoekstra, A. Y.: Benchmark levels for the consumptive water footprint of crop production for different environmental conditions: a case study for winter wheat in China, Hydrol. Earth Syst. Sci., 20, 4547-4559, https://doi.org/10.5194/hess-20-4547-2016, 2016b.

Zhuo, L., Mekonnen, M. M., Hoekstra, A. Y., and Wada, Y.: Inter-and intra-annual variation of water footprint of crops and blue water scarcity in the Yellow River basin (1961–2009), Adv. Water Resour., 87, 29-41, https://doi.org/10.1016/j.advwatres.2015.11.002, 2016c.